HHS Public Access

Author manuscript

J Extracell Biol. Author manuscript; available in PMC 2023 January 20.

Published in final edited form as:

J Extracell Biol. 2022 May ; 1(5): . doi:10.1002/jex2.43.

Biogenesis of JC polyomavirus associated extracellular vesicles

Jenna Morris-Love[1,2], **Bethany A. O'Hara**[2], **Gretchen V. Gee**[2,3], **Aisling S. Dugan**[4,5], **Ryan S. O'Rourke**[1,2], **Brandon E. Armstead**[1], **Benedetta Assetta**[2], **Sheila A. Haley**[2], **Walter J. Atwood**[2]

[1]Graduate Program in Pathobiology, Brown University, Providence, RI, USA

[2]Department of Molecular biology, Cellular Biology, and Biochemistry, Brown University, Providence, RI, USA

[3]MassBiologics, University of Massachusetts Medical School, Fall River, MA, USA

[4]Department of Biology, Assumption University, Worcester, MA, USA

[5]Department of Molecular Microbiology and Immunology, Brown University, Providence, RI, USA

Abstract

JC polyomavirus (JCPyV) is a small, non-enveloped virus that persists in the kidney in about half the adult population. In severely immune-compromised individuals JCPyV causes the neurodegenerative disease progressive multifocal leukoencephalopathy (PML) in the brain. JCPyV has been shown to infect cells by both direct and indirect mechanisms, the latter involving extracellular vesicle (EV) mediated infection. While direct mechanisms of infection are well studied indirect EV mediated mechanisms are poorly understood. Using a combination of chemical and genetic approaches we show that several overlapping intracellular pathways are responsible for the biogenesis of virus containing EV. Here we show that targeting neutral sphingomyelinase 2 (nSMase2) with the drug cambinol decreased the spread of JCPyV over several viral life cycles. Genetic depletion of nSMase2 by either shRNA or CRISPR/Cas9 reduced EV-mediated infection. Individual knockdown of seven ESCRT-related proteins including HGS, ALIX, TSG101, VPS25, VPS20, CHMP4A, and VPS4A did not significantly reduce JCPyV associated EV (JCPyV(+) EV) infectivity, whereas knockdown of the tetraspanins CD9 and CD81

Correspondence: Walter J. Atwood, Department of Molecular biology, Cellular Biology, and Biochemistry, Brown University, Providence, RI, USA. walter_atwood@brown.edu.

AUTHOR CONTRIBUTIONS

J.M-L. designed, performed, and analyzed experiments and wrote the manuscript. B.A.O. designed, performed, and analyzed initial cambinol experiments, aided in binding and uptake experiments, and edited the manuscript. G.V.G. designed, performed, and analyzed initial SMPD3 KO qPCR experiments, designed CD9, ALIX, and TSG101 shRNA sequences, mentored J.M-L., and edited the manuscript. A.S.D. designed and produced SMPD3 KO cell lines, and designed, performed, and analyzed initial experiments regarding nSMase2. R.S.O. performed Western blot in Suppl Fig 5B. B.E.A. cloned shRNA vectors CD9 and CD81. B.A. designed SMPD3 CRISPR/Cas9 with ASD. S.A.H. contributed to experimental design, support, and analysis and helped edit the manuscript. W.J.A. contributed to experimental design, support, and analysis, mentored J.M-L., edited the manuscript, and obtained funding to support the work.

CONFLICT OF INTEREST DISCLOSURE

No conflicts of interest are declared by the authors.

SUPPORTING IN FORMATION

Additional supporting information may be found in the online version of the article at the publisher's website.

or trafficking and/or secretory autophagy-related proteins RAB8A, RAB27A, and GRASP65 all significantly reduced the spread of JCPyV and decreased EV-mediated infection. These findings point to a role for exosomes and secretory autophagosomes in the biogenesis of JCPyV associated EVs with specific roles for nSMase2, CD9, CD81, RAB8A, RAB27A, and GRASP65 proteins.

Keywords

JC polyomavirus; extracellular vesicles; biogenesis

1 | INTRODUCTION

JC polyomavirus (JCPyV) is a non-enveloped human polyomavirus that establishes a lifelong and persistent infection in more than half the adult population (Egli et al., 2009; Ferenczy et al., 2012). Primary infection likely occurs during adolescence via the fecal-oral route and is generally asymptomatic (Bofill-Mas et al., 2001). However, JCPyV is the causative agent of the neurodegenerative disease progressive multifocal leukoencephalopathy (PML) (Adang & Berger, 2015; Assetta & Atwood, 2017; Atkinson & Atwood, 2020; Ferenczy et al., 2012; Torres, 2020). PML occurs in patients with severe immune-compromising conditions such as those with HIV/AIDS or in patients whose autoimmune disease is being treated with immune-modulatory drugs (Adang & Berger, 2015; Berger, 2017; Ferenczy et al., 2012; Major & Nath, 2016). While survival rates for PML patients have increased due to risk stratification and close patient monitoring, the survivors are often debilitated by this disease. No treatment options exist to treat or prevent JCPyV-induced PML other than restoring immune function that often leads to immune reconstitution syndrome and can be fatal if not properly managed (Adang & Berger, 2015; Berger, 2017; Cinque et al., 2009; Ferenczy et al., 2012).

JCPyV is known to infect cells by both receptor-dependent and receptor-independent mechanisms, the latter driven by extracellular vesicles (Assetta et al., 2013; Assetta et al., 2019; Elphick et al., 2004; Morris-Love et al., 2019; Neu et al., 2010; O'hara et al., 2020; Ströh et al., 2015). In receptor-dependent mechanisms, JCPyV first binds an attachment receptor known as lactoseries tetrasaccharide C, then interacts with entry receptor(s) 5-hydroxytryptamine type 2 (A, B, or C) for infectious entry (Assetta et al., 2013; Neu et al., 2010; Ströh et al., 2015). Extracellular vesicles describe a heterogeneous population of vesicles released from a cell including exosomes, microvesicles, secretory autophagosomes, and others. EVs can range in size from approximately 50 nm to 1000 nm (Claude-Taupin et al., 2017; Gudbergsson & Johnsen, 2019; Stoorvogel et al., 2002; Théry et al., 2002; Van Niel et al., 2018). EVs are crucial to health, normal function, and communication between cells but are also implicated in aiding many diseases and conditions like perpetuating cancer (Meldolesi, 2019; Xu et al., 2018), viral infections (Altan-Bonnet et al., 2019; Bello-Morales et al., 2018; English et al., 2009; Ghosh et al., 2020; Santiana et al., 2018; Schwab et al., 2015; Urbanelli et al., 2019; Van Der Grein et al., 2018), prion propagation (Abdulrahman et al., 2018; Chen et al., 2020; Rajendran et al., 2006; Vella et al., 2007), inflammation (Abbott, 2002; Balusu et al., 2016; Datta Chaudhuri et al., 2020; Soria et al., 2017), and neurodegeneration (Frühbeis et al., 2013; Hu et al., 2016; Soria et al., 2017; You &

Ikezu, 2019). The spread of non-enveloped viruses by extracellular vesicles is of particular interest as more and more research show viruses can infect in a typical receptor-dependent mechanism but also an EV-mediated, receptor-independent mechanism (Kerviel et al., 2021; Santiana et al., 2018). Many studies have sought to understand the biogenesis pathways required to produce different types of EVs and yielded interesting, sometimes seemingly contradictory results that contribute to the intricate web of mechanisms producing EVs (Stoorvogel et al., 2002; Théry et al., 2002; Van Niel et al., 2018). Pathogens can also alter biogenesis pathways adding to the complexity of understanding EV biogenesis in the context of infection (Jia et al., 2021; Martins & Alves, 2020; Pleet et al., 2018).

In this article we aimed to evaluate major EV biogenesis pathways that contribute to the production of JCPyV associated exosomes, microvesicles, and/or secretory autophagosomes. Exosomes are produced by several pathways often broadly characterized as ESCRT-independent and ESCRT-dependent (Colombo et al., 2014; Stoorvogel et al., 2002; Théry et al., 2002; Van Niel et al., 2018). Endosomal sorting complexes required for transport (ESCRT)-independent methods include neutral sphingomyelinase 2 (nSMase2) (Menck et al., 2017; Trajkovic et al., 2008; Verderio et al., 2018) and tetraspanins (Andreu & Yáñez-Mó, 2014; Charrin et al., 2014; Dogrammatzis et al., 2019; Van Niel et al., 2011). nSMase2 cleaves sphingomyelin to phospholipids and ceramide at endosomal membranes. The structure of ceramide can induce negative membrane curvature (Goñi & Alonso, 2009), producing intraluminal vesicles within the endosome and creating a multivesicular body (MVB). Some of the most common EV markers include the tetraspanins CD9, CD81, and CD63 for their clear enrichment in EVs (Witwer et al., 2017). The structure of tetraspanins allow these proteins to dimerize and form tetraspanin-enriched microdomains and interact with an assortment of other proteins forming complex protein networks (Andreu & Yáñez-Mó, 2014; Umeda et al., 2020; Zimmerman et al., 2016). Tetraspanins are implicated in cargo sorting and loading into vesicles, targeting to distal cells for uptake, and MVB formation by inducing membrane curvature (Andreu & Yáñez-Mó, 2014; Gordón-Alonso et al., 2006; Snead et al., 2017; Stachowiak et al., 2012; Umeda et al., 2020; Van Niel et al., 2011; Zimmerman et al., 2016). Alternatively, an ESCRT-dependent mechanism of MVB formation encompasses the complex ESCRT machinery and ESCRT accessory proteins that aid in cargo sorting and loading, membrane invagination, and membrane scission (Colombo et al., 2013; Henne et al., 2011; Im et al., 2009; Juan & Fürthauer, 2018; Schmidt & Teis, 2012; Wollert & Hurley, 2010). ESCRTs can also produce microvesicles that bud directly from the plasma membrane (Colombo et al., 2013; Fujii et al., 2007; Juan & Fürthauer, 2018; Wollert & Hurley, 2010). After formation, MVBs can traffic to the plasma membrane for fusion and release the internal vesicles (exosomes) to the extracellular space (Menck et al., 2017; Shamseddine et al., 2015; Trajkovic et al., 2008; Verderio et al., 2018). MVBs can also be targeted for degradation via a lysosomal pathway or fused with an autophagosome to create an amphisome. Amphisomes can similarly be targeted for degradation or an unconventional secretion method (Claude-Taupin et al., 2017; Fader et al., 2008; Ponpuak et al., 2015). Trafficking of MVBs and amphisomes to the plasma membrane is controlled by the small GTPase RAB27A (Chen et al., 2017; Ostrowski et al., 2010). Autophagosome formation is a highly regulated process involving a series of proteins and protein complexes that induce double membrane phagophore formation, extension, and maturation into a

complete, cargo-loaded vesicle (Hurley & Young, 2017; Yu et al., 2018). Autophagosomes are targeted for degradation via lysosomal fusion to form an autophagolysosome or enter unconventional secretion pathways (Claude-Taupin et al., 2017; Hurley & Young, 2017; Ponpuak et al., 2015; Yu et al., 2018). The small GTPase RAB8A and Golgi re-assembly and stacking proteins (abbrev. GRASP or GoRASP) GRASP55/GoRASP2 and GRASP65/GoRASP1 have been implicated in unconventional secretion pathways (Baixauli et al., 2014; Claude-Taupin et al., 2017; Dupont et al., 2011; Pleet et al., 2018; Ponpuak et al., 2015; Tancini et al., 2019; Zhang & Schekman, 2013; Zhang et al., 2015). RAB8A has been studied as a key mediator of trafficking autophagosomes to the plasma membrane as shown during unconventional secretion of IL-1β (Dupont et al., 2011), whereas the isoform RAB8B appears to be more important for degradation of autophagosomes, as noted in a macrophage system (Pilli et al., 2012). GRASPs function to maintain the integrity of Golgi stacks, with GRASP55 localized mostly at the medial and trans Golgi, and GRASP65 the cis Golgi (Bekier et al., 2017; Feng et al., 2013; Tang et al., 2010; Veenendaal et al., 2014; Xiang & Wang, 2010; Zhang & Seemann, 2021; Zhang & Wang, 2020). Under stress conditions, GRASPs can relocalize to other membranes like the endoplasmic reticulum (ER) or plasma membrane (Giuliani et al., 2011). GRASPs have been implicated in unconventional protein secretion (UPS) of cystic fibrosis transmembrane conductance regulator (CFTR), IL-1β, and insulin-degrading enzyme in mammalian systems (Dupont et al., 2011; Gee et al., 2011; Son et al., 2016; Zhang et al., 2015). Other species models have found GRASPs contribute to UPS of acyl-CoA binding protein (AcbA) in *Dictyostelium* (amoeba) and some yeast models, and αPS2 integrin in Drosophila models (Mendes et al., 2019; Rabouille, 2017). Human GRASP55 was also recently shown to contribute to autophagosome-lysosome fusion (Zhang et al., 2019; Zhang et al., 2018). It is imperative to note that while many proteins are attributed to specific pathways, these proteins have multiple functions and localizations depending on cell status, and there is a high degree of overlap amongst the exocytic pathways.

Here we unravel mechanisms contributing to virus-EV biogenesis. We evaluated the role of ESCRT-independent and - dependent mechanisms that produce exosomes, including nSMase2, tetraspanins, and ESCRT proteins, and secretory autophagosomes in the production of JCPyV(+) extracellular vesicles. We found that inhibiting or depleting nSMase2 prevents the spread of JCPyV over several infection cycles and genetic depletion produces less infectious virus(+) EVs. This defect is consistent with a decrease in virus-EV association, suggesting virus can use the exosomal pathway. Knockdown of the tetraspanins CD9 or CD81 similarly reduced the spread of virus and produced less infectious EVs. Meanwhile, ESCRT-dependent EV production did not seem to play a role in JCPyV(+) EV production as knockdown of seven related proteins did not reduce the spread of virus or EV-mediated infection. Finally, it was discovered that knockdown of proteins RAB8A, RAB27A, and GRASP65 that are implicated in secretory autophagy reduced the spread of virus and EV-mediated infection. This indicates secretory autophagosomes and amphisomes also contribute to the JCPyV(+) EV population. Overall our data indicate a specific role for ESCRT-independent exosome production and secretory autophagosomes in the biogenesis of JCPyV(+) EVs.

2 | MATERIALS AND METHODS

2.1 | Cells and viruses

SVG-A is a transformed cell line derived from primary fetal human glial cells and was described previously (Major et al., 1985). SVG-A cells were grown in minimal essential medium (MEM) (Corning, Inc, New York, NY) supplemented with 10% fetal bovine serum (FBS) (Atlanta Biologicals, Flowery Branch, GA) and 1% antifungal/antibiotic (Gibco Life Technologies, Gaithersburg, MD). HEK293-LentiX cells are a subclone of the HEK293 line optimal for lentiviral packaging systems and were obtained from (Takara). LentiX cells were grown in Dulbecco's minimal essential medium (DMEM) (Corning) supplemented with 10% FBS, 1% nonessential amino acids (Gibco Life Technologies), and 1% antifungal/antibiotic. EV-depleted media was used as needed for EV-related experiments while complete media was used for general passage of cell lines. EV-depleted media was produced as described (Théry et al., 2002). Briefly, 2X media was prepared and spun at 100,000 ×g in a Type 45 Ti rotor (k-factor = 133), for 18 hours at 4°C. Media was then diluted before use to 1X and filtered through 0.22 μm filter (CELLTREAT, Pepperell, MA). Cells were grown in a humidified chamber at 37°C and 5% CO_2.

Generation of the JC polyomavirus strain Mad-1/SVEΔ and production and purification of viral stocks was previously described (Liu & Atwood, 2000, Liu et al.).

2.2 | Antibodies and reagents

Primary antibodies and respective dilutions for Western blots include annexin V (Abcam, Cambridge, UK ab117439, 1:1000), CD9 (Cell Signaling Techologies, Danvers, MA, CST 13174S, 1:1000), CD81 (Systems Biosciences, Palo Alto, CA, 1:1000), Flotillin-1 (CST 18634S, 1:1000), ALIX (CST 3A9, 1:1000) or (CST E6P9B, 1:1000), GRASP65 (Thermo PA3910, 1:5000), RAB8A (CST D22D8, 1:1000), RAB27A (CST D7Z9Q, 1:1000), LC3A/B (CST D3U4C, 1:1000), β-actin (CST 8H10D10, 1:1000), and PAB597 (purified, 1:2000). PAB597 is a monoclonal antibody against VP1 (Atwood et al., 1995). Secondary antibodies for Western blots include anti-Mus-HRP (Thermo A28177) and anti-Rabbit-HRP (Thermo A27036) both used at 1:10,000. Anti-rabbit-680, anti-mouse-680, anti-rabbit-800, and anti-mouse-800 (Li-Cor, Lincoln, NE) all used at 1:5,000.

2.3 | shRNA vectors

Generation of all shRNA vectors was completed as described (https://www.addgene.org/protocols/plko/) for plKO.1 vectors (Addgene, (Moffat et al., 2006)). shRNA sequences were chosen from the RNAi Consortium (http://www.broad.mit.edu/genome_bio/trc/rnai.html) and are listed below. Sequences were ordered from IDTDNA.

Target	Sequence (5′ → 3′)
SMPD3 Sense	CCGGCCAAAGAATCGTCGGGTACATCTCGAGATGTACCCGACGATTCTTTGGTTTTTG
SMPD3 Antisense	AATTCAAAAACCAAAGAATCGTCGGGTACATCTCGAGATGTACCCGACGATTCTTTGG

Target	Sequence (5′ → 3′)
CD9 Sense	CCGGCGCGAGATGGTCTAGAGTCAGCTTACTCG AGTAAGCTGACTCTAGACCATCTCGCGTTTTTG
CD9 Antisense	AATTCAAAAACGCGAGATGGTCTAGAGTCAGCTTACTCGAGTAAGCTGACTCTAGACCATCTCGCG
CD81 Sense	CCGG CACATGTAGGTGGCGTGTATG CTCGAG CATACACGCCACCTACATGTG TTTTTG
CD81 Antisense	AATTCAAAAACACATGTAGGTGGCGTGTATG CTCGAG CATACACGCCACCTACATGTG
HGS Sense	CCGGGTGAGCCACAGTTCCACAATGCTCGAGCATTGTGGAACTGTGGCTCACTTTTTG
HGS Antisense	AATTCAAAAAGTGAGCCACAGTTCCACAATGCTCGAGCATTGTGGAACTGTGGCTCAC
ALIX Sense	CCGGGGAAGGATGCTTTCGATAAAGGTTCCTCGAGGAACCTTTATCGAAAGCATCCTTCCTTTTTG
ALIX Antisense	AATTCAAAAAGGAAGGATGCTTTCGATAAAGGTTCCTCGAGGAACCTTTATCGAAAGCATCCTTCC
TSG101 Sense	CCGGGTTTATCATTCAAGTGTAAAATATTCTCGAGAATATTTTACACTTGAATGATAAACTTTTTG
TSG101 Antisense	AATTCAAAAAGTTTATCATTCAAGTGTAAAATATTCTCGAGAATATTTTACACTTGAATGATAAAC
VPS25 Sense	CCGGGAGTCGATCCAGATTGTATTACTCGAGTAATACAATCTGGATCGACTCTTTTTG
VPS25 Antisense	AATTCAAAAAGAGTCGATCCAGATTGTATTACTCGAGTAATACAATCTGGATCGACTC
VPS20 Sense	CCGGGTGGAGTACCAGCGGCAAATACTCGAGTATTTGCCGCTGGTACTCCACTTTTTG
VPS20 Antisense	AATTCAAAAAGTGGAGTACCAGCGGCAAATACTCGAGTATTTGCCGCTGGTACTCCAC
CHMP4A Sense	CCGGCACAAACTGACGGGACATTATCTCGAGATAATGTCCCGTCAGTTTGTGTTTTTG
CHMP4A Antisense	AATTCAAAAACACAAACTGACGGGACATTATCTCGAGATAATGTCCCGTCAGTTTGTG
VPS4A Sense	CCGGCGAGAAGCTGAAGGATTATTTCTCGAGAAATAATCCTTCAGCTTCTCGTTTTTG
VPS4A Antisense	AATTCAAAAACGAGAAGCTGAAGGATTATTTCTCGAGAAATAATCCTTCAGCTTCTCG
RAB8A Sense	CCGGCTCGATGGCAAGAGAATTAAACTCGAGTTTAATTCTCTTGCCATCGAGTTTTTG
RAB8A Antisense	AATTCAAAAACTCGATGGCAAGAGAATTAAACTCGAGTTTAATTCTCTTGCCATCGAG
RAB27A Sense	CCGGCCAGTGTACTTTACCAATATACTCGAGTATATTGGTAAAGTACACTGGTTTTTG
RAB27A Antisense	AATTCAAAAACCAGTGTACTTTACCAATATACTCGAGTATATTGGTAAAGTACACTGG
GRASP65 Sense	CCGGCGTGTCGGGAATTTCTCTCTTCTCGAGAAGAGAGAAATTCCCGACACGTTTTTG
GRASP65 Antisense	AATTCAAAAACGTGTCGGGAATTTCTCTCTTCTCGAGAAGAGAGAAATTCCCGACACG

2.4 | Generation of CRISPR knockout cell lines

SMPD3 CRISPR/Cas-9 knockout cells were generated using the guidelines provided by www.crispr.mit.edu. Guide oligos were designed using the MIT CRISPR database. The oligo and complement chosen were

SMPD3-F 5′-CACCGTGGCGCTTCTCGTAGGTGGT-3′ and SMPD3-R 5′-AAACACCACCTACGAGAAGCGCCAC-3′. The oligos were cloned into LentiCRISPR.v2 (AddGene). Lentivirus was produced using LentiX 293T cells and the packaging plasmid pCMV-dr8.91 (AddGene) and envelope plasmid VSV-G (AddGene) with the designed guide DNA LentiCRISPR plasmid. Lentivirus was filtered through 0.45μm filter (Millipore) and supplemented with 8 μg/mL polybrene. Complete lentivirus was used to transduce SVG-A with three serial 24 hour infections. Transduced cells were then selected with 2 μg/mL puromycin. This is the mixed population of CRISPR clones. Single clones were picked using cell rafts (Cell Microsystems) and the QIAscout system (QIAGEN). Clones were expanded from a 96 well plate and sequences confirmed according to MGH CRISPR Amplicon sequencing guidelines (www.dnacore.mgh.harvard.edu). Primer pair sets for the SMPD3 gene are as follows: Fwd1 5′-GTGTGTCCTGGGCCCTTATC-3′, Rev1 5′-GGGGACCAGAAGAGAAAGCC-3′ and Fwd2 5′-CTAACAGCTGTCTGTCCGCC-3′, Rev2 5′-AGAGAAAGCCGAGAAACGCA-3′.

2.5 | Production and purification of extracellular vesicles

Cells were plated at 10,000 cells/cm^2 and infected for 2 hours in serum-free media using purified JC polyomavirus at an MOI of 100 viral genomes/cell. After infection, inoculum was aspirated and replaced with complete, EV-depleted media. Supernatants were collected at 7 dpi. At time of harvest, cells were trypsinized and counted using a CellCountess (Thermo) cell counter and viability was noted. If cell viability was greater than or equal to 95%, the supernatant was used for EV purification.

EVs were produced by differential centrifugation, first pelleting out debris at 300 ×g in a Sorvall Legend X1R (Thermo) centrifuge for 10 min, decanted to a fresh tube and spun at 2,000 ×g for 10 min. Supernatant was decanted to a fresh tube and spun at 10,000 ×g in a Sorvall Lynx 6000 (Thermo) centrifuge for 30 min 2x. Supernatant was decanted to UltraClear tubes (Beckman Coulter, Brea, CA) and spun at 100,000 ×g for 70 min in a SW55 Ti rotor (*k*-factor = 139) or 2 hr 10 min in a SW41 Ti rotor (*k*-factor = 256). The pellet was washed with PBS and re-pelleted at 100,000 ×g. The pellet was resuspended in sterile PBS at 1/100th the starting volume and stored at 4°C for short-term storage or −20°C for long-term storage. All spins were carried out at 4°C. EV preps were evaluated by Western, TEM, NTA, qPCR, and/or protein and DNA concentration by Qubit analysis. Generally, EV preps were characterized and used within 1 week of production or frozen.

It is important to note that JCPyV in the supernatant can co-purify with EVs so JCPyV(+) EVs are a heterogeneous population containing virus(+) EVs with varying degrees of association. This can include free virus, JCPyV positive EVs, and ‘empty’ (JCPyV negative) EVs.

2.6 | Western blot analysis

Whole cell lysate (WCL) samples were lysed on ice in Pierce RIPA buffer (Thermo) supplemented with cOmplete EDTA-free protease inhibitor cocktail (Roche). Extracellular vesicle samples were resuspended in phosphate buffered saline (PBS) or buffer A supplemented with 2.5% deoxycholate (DOC) and 0.01% triton X and supplemented with

cOmplete EDTA-free protease inhibitor cocktail, followed by 3 freeze thaws. Protein content for WCL and EV (DOC-containing buffer) samples was determined by Peirce Rapid Gold BCA Protein Assay kit (Thermo) according to manufacturer's protocol. Protein content of EV (in PBS) was determined using a Qubit Fluorometer according to manufacturer's protocols. All samples were prepared in 4X loading dye (Bio-Rad Laboratories, Hercules, CA) supplemented with beta-mercaptoethanol (Bio-Rad), boiled at 95°C for 5 min, briefly spun down and incubated on ice before being loaded into 4–15% gradient Mini-Protean TGX Stain-Free pre-cast gels (Bio-Rad). Stain-Free gels were run at 150–200V and activated and imaged on a ChemiDoc MP Imaging System (Bio-Rad), then transferred to a 0.2 μm nitrocellulose membrane by the semi-dry transfer method. After transfer, Stain-Free gels were reimaged to determine efficiency of protein transfer, and blots were blocked in 1% casein buffer in Tris Buffered Saline (TBS) (Bio-Rad). Primary antibodies were diluted in 1% casein and incubated overnight at 4°C on a rocker. Blots were washed 3X with TBS with 0.01% Tween-20 (TBSt) and incubated with secondary antibody diluted in TBSt for 1 hour at room temperature with rocking. Horseradish protein (HRP) secondary antibodies were diluted 1:10,000 and fluorescent secondary antibodies were diluted 1:5,000. Blots were washed 3X with TBSt, then incubated with ClarityMax according to manufacturer's protocols (Bio-Rad) for HRP secondary antibodies. Blots were imaged on a ChemiDoc MP Imaging System.

2.7 | Nanoparticle tracking analysis

Nanoparticle tracking analysis (NTA) was performed using a Malvern Nanosight NS300 or Particle Metrix Zetaview Quatt. When using the Malvern system, samples and standards were diluted in PBS. Nanosphere bead standards (Thermo) were diluted to 1:1000 and 1:10,000 and used to focus the NTA reading, followed by a thorough wash with degassed PBS. After each sample, the nanosight lines were thoroughly washed. Parameters were set as follows: flow rate of 50 μL/min, with five 30 s videos recorded for analysis.

For the Particle Metrix system, nanoparticle tracking analysis was completed according to manufacturer's recommended protocol. Briefly, polystyrene beads were diluted in Milli-Q (MQ) water upon start-up for optimal focus. Samples were diluted in MQ water and examined at 11 separate positions. Each sample was followed by a thorough wash with MQ water. Size distributions from were overlayed in FlowJo.

All NTA data is represented as particles produced per cell by dividing the total particles (found by NTA) over the total cell count data (taken at time of harvest). This normalization method was chosen to compare across genetic backgrounds.

2.8 | Viral spread assays

Cells were plated at a density of 5,000 cells/cm^2 and infected for 2 hours in serum-free media using purified JC polyomavirus at an MOI of 200 viral genomes/cell (determined using qPCR). Inoculum was removed and cells washed with 1x PBS, before adding excess EV-depleted media (200 μL for 96w format and 1 mL for 24w format) and fixed for indirect immunofluorescence analysis at 3, 6, or 9 days post infection (dpi). At 6 dpi, extra

EV-depleted media was added to cells (50 μL for 96w format and 0.5 mL for 24w format) to prevent starvation-induced pathways and acidification.

2.9 | EV reinfection assays

Cells were plated at a density of 10,000 cells/cm^2. EV samples were diluted 1:10 in serum-free media and adsorbed to naïve SVG-A cells for 2 hours at 37°C. Inoculum was aspirated and replaced with EV-depleted media. Cells were incubated at 37°C and 5% CO_2 for 3 days, then fixed for indirect immunofluorescence analysis as described below.

2.10 | qPCR: EV treatments and DNA purification

Before DNA purification, EVs were treated with DNaseI to remove free, non-encapsidated viral genomes. DNaseI (NEB) was added to a final concentration of 120 Units/mL to the EVs, mixed, and incubated on a shaking heat block set to 37°C and 300 rpm for 1 hr. DNaseI was then inactivated by incubating at 75°C for 10 min. DNA was purified from the treated samples using the Blood & Tissue DNA Purification Kit (QIAGEN) according to manufacturer's protocols.

DNA purification of JCPyV viral genomes from whole cell lysates (WCL) was completed using the Blood & Tissue DNA Purification kit without pretreatment. DNA concentration for WCL was determined via Nanodrop 2000 (Thermo).

2.11 | Quantitative PCR

Viral genomes were quantified using qPCR. Plasmid DNA containing the full JCPyV genome was used to create a standard curve for absolute genome quantification. Primer/probe sets targeting VP2 (Primer 1: 5′-CCTGGAGTGAATGCCTTTGT-3′, Primer 2: 5′-AGAGGTTAAGGCTGGCAAATC-3′, Probe: 5′TGTTCTCCACAATCTCCCAGGCTT-3′) or VP1 (Primer 1: 5′-CAGCCTCCCACATGAGTATATTT-3′, Primer 2: 5′-AGGGACATGCTTCCTTGTTAC-3′, Probe: 5′-TGTGGCCAGAATTCCACTACCCAA-3′) were ordered from IDTDNA. Samples were prepared using the PrimeTime 2X master mix (IDTDNA) according to manufacturer's protocols and run on a CFX96 qPCR detection system (BioRad).

2.12 | RT-qPCR

RT-qPCR was used to confirm knockdown of gene expression. RNA was purified from cells using the RNeasy Mini Kit (QIAGEN) according to the manufacturer's protocol, including the additional DNase step. cDNA was created using 500 ng of RNA with the iSCRIPT cDNA synthesis kit (BioRad) according to the manufacturer's protocol and used directly for the qPCR reaction. Relative gene expression was determined using the $2^{\Delta\Delta Ct}$ values, normalizing to GAPDH or β-actin. Primer/probe sets were purchased from IDTDNA and the corresponding assay numbers are listed in the following table:

Primer/Probe Set		
SMDP3	Primer 1:	GGTCCTGAGGTGTGCTTC

Primer/Probe Set		
	Primer 2:	TCTTTGCCAGCCGCTAC
	Probe	/56-FAM/ACCTGCACC/ZEN/TTGAGAAACAGAGCTC/3IABkFQ/
	IDT Assay:	Hs.PT.58.38391129
CD9	Primer 1:	GTTTCTTGCTCGAAGATGCTC
	Primer 2:	CACCAAGTGCATCAAATACCTG
	Probe	/56-FAM/AATCCCGGC/ZEN/AAGCCAGAAGATGA/3IABkFQ/
	IDT Assay:	Hs.PT.56a.4183031
CD81	Primer 1:	TCTCCCAGCTCCAGATACAG
	Primer 2:	GCTCTTCGTCTTCAATTTCGTC
	Probe	/56-FAM/CCATGACCC/ZEN/GCAGACCACCAA/3IABkFQ/
	IDT Assay:	Hs.PT.58.454503
HGS	Primer 1:	CCTCCACTTGTCTCTTCAGC
	Primer 2:	ACGTCGCCTTGTATGCC
	Probe	/56-FAM/TCCTCCATG/ZEN/GTCTGCTTGTTGGC/3IABkFQ/
	IDT Assay:	Hs.PT.58.40180026
ALIX	Primer 1:	CTGTTCTGCTGCAATTTGGC
	Primer 2:	AGGTTCACTTTTTGGAGGCT
	Probe	/56-FAM/TGAAAAGAG/ZEN/CTGTGTGTTGTTCAATTGTGC/3IABkFQ/
	IDT Assay:	Hs.PT.58.20433720
TSG101	Primer 1:	TGACCGCAGAGATGAGAGAG
	Primer 2:	TCCATATCCTGCCACAACAAG
	Probe	/56-FAM/ACAATCAGC/ZEN/GAGGACACCATCCG/3IABkFQ/
	IDT Assay:	Hs.PT.58.22485669
VPS25	Primer 1:	TCCTCATCCTCTGTGTCTTCC
	Primer 2:	GTCCAGCTTCCTGATCATGT
	Probe	/56-FAM/CTATCAGTG/ZEN/GGTTTCCAGGAGTGGC/3IABkFQ/
	IDT Assay:	Hs.PT.58.4211667
VPS20	Primer 1:	GTACTGCCTCAGCTTGTCC
	Primer 2:	GTGGCGATTGGACTTGGT
	Probe	/56-FAM/CTTCAGTTG/ZEN/CAGGATGGCCTTGTC/3IABkFQ/
	IDT Assay:	Hs.PT.58.4652164
CHMP4A	Primer 1:	CTCCAGCAGTTCATCCTCATC
	Primer 2:	AGAAGGCCTACCAGGACAT
	Probe	/56-FAM/CCCAGCAGA/ZEN/TCTCAGATGCCATTTCT/3IABkFQ/
	IDT Assay:	Hs.PT.58.22796991
VPS4A	Primer 1:	CTCGTAGTTCTTGGCTTTGTC
	Primer 2:	GGACCCAGGAGATGAAATGAC
	Probe	/56-FAM/TCAATGGCT/ZEN/TTCTGGAGGGTTGACG/3IABkFQ/
	IDT Assay:	Hs.PT.58.15677403
RAB8A	Primer 1:	CAATGTTGCGAATCCAGTTCC
	Primer 2:	GATCACAACGGCCTACTACAG
	Probe	/56-FAM/CATCACCAA/ZEN/CGAGAAGTCCTTCGACA/3IABkFQ/

Primer/Probe Set		
	IDT Assay:	Hs.PT.58.1211675
RAB27A	Primer 1:	TAACTGCAGGTGGATTCTCTG
	Primer 2:	CAACAGTGGGCATTGATTTCAG
	Probe	/56-FAM/AGAGTGGTG/ZEN/TACAGAGCCAGTGGG/3IABkFQ/
	IDT Assay:	Hs.PT.58.40278217
GRASP65	Primer 1:	TCATATTGAACACCTCCAGCTT
	Primer 2:	GGAGCCCTACTTTGACTTCATC
	Probe	/56-FAM/ACACCCTGA/ZEN/AGGCACTACTGAAAGC/3IABkFQ/
	IDT Assay:	Hs.PT.58.20540327
GAPDH	Primer 1:	TGTAGTTGAGGTCAATGAAGGG
	Primer 2:	ACATCGCTCAGACACCATG
	Probe	/5HEX/AAGGTCGGA/ZEN/GTCAACGGATTTGGTC/3IABkFQ/
	IDT Assay:	Hs.PT.39a.22214836
B-Actin	Primer 1:	CCTTGCACATGCCGGAG
	Primer 2:	ACAGAGCCTCGCCTTTG
	Probe	/56-FAM/TCATCCATG/ZEN/GTGAGCTGGCGG/3IABkFQ/
	IDT Assay:	Hs.PT.39a.22214847

2.13 | MTS assay

Cytotoxicity of cambinol (Sigma) was determined using the CellTiter 96® AQ_{ueous} One Solution Cell Proliferation Assay (Promega) according to manufacturer's protocols. Briefly, SVG-A cells were plated in complete media. The next day, cells were treated with cambinol diluted to several concentrations in complete media, or a volume-matched vehicle control at the highest concentration. At 3, 6, or 9 days post drug treatment, MTS reagent was added for 1–4 hrs and absorbance read at 450 nm using a Glomax Multi Detection System (Promega) plate reader. At 6 days post infection (dpi), additional media with drug or vehicle control was added to cells at the same final concentration

2.14 | Drug treatments

Cambinol (Sigma) was resuspended in DMSO to a stock concentration of 1 mM. For the cambinol experiments, cells were first infected with purified JCPyV in serum-free media (SFM). After 2 hr virus inoculum was removed and cells were washed with 1X PBS, then complete EV-depleted media with 10 μM cambinol or a volume-matched vehicle control was added. At 6 days post infection (dpi), additional media with drug or vehicle control was added to cells at the same final concentration (96w format – 50 μL; 24w format – 0.5 mL).

2.15 | Labeling EVs

EVs were labeled using PKH67 lipophilic dye (Sigma) according to manufacturer's protocols with slight variations. Briefly, EVs were diluted in the provided Diluent C to 1 mL in UltraClear ultracentrifuge tubes (Beckman Coulter, fit SW41Ti rotor). 6 μL of PKH67 was added to the diluted EVs and gently mixed by pipetting for 30 seconds. The labeling reaction was allowed to proceed for 5 minutes, then 8–10 mL of EV-depleted media was

added to stop the reaction. 1X PBS was added to each sample to bring the volume up to 12 mL, then samples were spun at 28,500 rpm for 130 minutes (*k*-factor = 257). Labeled EVs were resuspended in 1XPBS, evaluated for particle concentration using the Zetaview NTA system, and samples were further diluted in 1XPBS maintaining the ratio of particles/mL determined by NTA so all samples would have the same particle concentration in an equal volume. Dye label controls included equal volumes of PBS and/or EV-depleted media in place of EVs in the labeling reaction. The dye control with the higher %PKH67(+) signal was used for analysis.

2.16 | Uptake experiments (flow cytometry)

Cells were plated at a density of 20,000 cells/cm^2 in 24w plates with complete media. The next day, cells were serum-starved and pre-chilled at 4°C for 30–60 min. Labeled EVs were added at equal concentrations to each well in ice-cold serum-free media or 1XPBS and allowed to bind for 60 min at 4°C. Plates were then shifted to 37°C for 2 hr to allow for uptake. After uptake, cells were washed, trypsinized, and resuspended in complete media. Cells were spun down, washed with 1XPBS, spun down again, and resuspended in 250–350 μL PBS. Samples were read using a BD FACS CantoII flow cytometer to get an initial reading. Then trypan blue was added to a final concentration of 0.008% to quench any external fluorescent signal and read again to evaluate internalized EV signal. FlowJo was used to analyze flow cytometry data to first gate on cells based on the side scatter against forward scatter. The gated cell population was then evaluated for PKH67(+) and PKH67(−) signal based on the highest positive dye label control and is represented as percent of (gated) parent cell population.

2.17 | Indirect immunofluorescence analysis

Cells were fixed and permeabilized in 100% methanol for 30 min at −20°C. After fixation cells were blocked with 10% goat serum in PBS for 45 min. Anti-VP1 antibody (PAB597) was diluted 1:50 in PBS and incubated on cells for 1–1.5 hours at 37°C. Cells were washed 3X with PBS. Goat anti-mouse secondary conjugated with Alexa-488 Flour or Alexa-594 Fluor was diluted 1:500 in PBS and incubated on cells for 1 hr at 37°C. Cells were washed 3X with PBS, then incubated with DAPI diluted 1:1000 in PBS for 10 min. Cells were washed 2X and imaged on a Nikon Ti2E Fluorescence Microscope using a 20X objective. Analysis of images was done using the Nikon High Content Imaging Software to count DAPI-positive and VP1-positive nuclei. Percent VP1(+) cells was calculated for analysis.

2.18 | Statistical analysis

All experiments were completed in triplicate and repeated 3 times unless noted otherwise in the figure legend. GraphPad Prism 9 was used for graphing and statistical analyses to determine significant changes between control and treatment samples. Statistical tests include unpaired t tests (against respective CTRL or WT), one-way ANOVA with Dunnet's method (EV-reinfections with 3+ conditions), two-way ANOVA (viral spread, qPCR viral genomes in WCL vs EV) with Dunnett's method for multiple comparisons. p-values are designated as follows *$p < 0.05$, **$p < 0.01$, ***$p < 0.001$, ****$p < 0.0001$, ns $p > 0.05$. Unless specified, graphs represent the mean and standard error calculated from samples.

3 | RESULTS

3.1 | Disruption of neutral sphingomyelinase 2 reduces EV-mediated spread of JCPyV

Infectious spread of JCPyV may occur by virus-, cell-to-cell-, and/or EV-mediated entry to target cells. To understand the role of exosomes in the spread of JCPyV by extracellular vesicles we first evaluated the role of neutral sphingomyelinase 2 (nSMase2). SVG-A cells were infected with JCPyV then treated with either vehicle control or the nSMase2 inhibitor cambinol (Figuera-Losada et al., 2015) at a non-toxic dose to the cells (Supplementary Fig 1A) and evaluated for viral spread over several infection cycles. By 9 days post infection (dpi) JCPyV spread was significantly reduced in cambinol treated cells compared to vehicle control (Fig 1A). Importantly, there was no significant reduction during the initial viral life cycle (3 dpi), indicating there is no inhibitory action by the drug to early viral infection. This demonstrates that nSMase2 inhibition results in fewer infected cells, implying exosomes contribute to viral spread. It is important to note that cambinol is a known inhibitor of sirtuin (SIRT) 1 and 2 with an IC50 of approximately 56 and 59 μM, respectively (Heltweg et al., 2006). Though the concentration used here is lower, we cannot exclude the possibility off-target effects of the drug on JCPyV mediated infection.

We proceeded to knockdown nSMase2 using shRNA to target the nSMase2-encoding gene sphingomyelinase phosphodiesterase 3 (SMPD3) and produce stable cell lines. Knockdown of SMPD3 expression was confirmed using RT-qPCR (Fig 1B) compared to the shRNA control cell line. SMPD3 knockdown (KD) or control (CTRL) cells were infected with JCPyV and evaluated for viral spread over 9 days. Early infection (3 dpi) was not altered by SMPD3 KD but viral spread was significantly reduced by 9 dpi compared to CTRL cells (Fig 1C). To evaluate whether this reduction in spread was due to decreased production of JCPyV(+) EVs, EVs were concentrated from the supernatant of infected cells and characterized using nanoparticle tracking analysis (NTA), transmission electron microscopy (TEM), and Western blot analysis for EV markers and the absence of non-EV markers. Characterization revealed that SMPD3 KD cells produced more particles per cell by NTA compared to CTRL EVs, but size distribution was unchanged (Fig 1D, Supplementary Fig 1B). TEM showed all EVs retained similar morphology and demonstrated virus was associated with EVs regardless of genetic background (Fig 1E, Supplementary Fig 1C, D). Western blot analysis confirmed the presence of typical EV markers like CD9, FLOTILLIN-1, ALIX, and ANNEXIN V across CTRL and SMPD3 KD EVs while potential cell contaminants like GM130 were absent from the EVs compared to the whole cell lysate (WCL) (Fig 1F). An EV-reinfection assay revealed JCPyV(+) EVs derived from SMPD3 KD cells were significantly less infectious than those derived from CTRL cells (Fig 1G). To determine whether there were fewer viral particles packaged into the EVs in the absence of nSMase2, quantitative PCR was used to measure total viral genomes in the whole cell lysate (WCL) and protected, or encapsidated, viral genomes associated with EVs. Interestingly, qPCR did not reveal significant changes in viral genomes associated with EVs between SMPD3 KD and CTRL (Fig 1H), nor was there a significant change between total viral genomes in the WCL (Supplementary Fig 1E). To determine if the reduction in EV-mediated infection might result from a binding or entry defect, JCPyV(+) EVs derived from CTRL or SMPD3 KD cells were labeled with the lipophilic dye PKH67 and incubated with cells at

4°C to bind EVs to target cells, then shifted to 37°C for internalization. PKH67(+) cells were detected by flow cytometry before and after a trypan blue quench step to evaluate total and protected PKH67 (internalized EV) signal. There was no binding defect (data not shown) or internalization defect detected (Fig 1I).

Overall these data show that SMPD3 KD cells produced less infectious EVs than CTRL cells even though the EVs contained the same quantity of encapsidated viral genomes. We considered this might be one of two possibilities—a result of incomplete genetic depletion and therefore incomplete protein disruption of nSMase2 and/or other EV producing pathways can compensate for the depletion of nSMase2 thereby allowing for sufficient virus(+) EV release. We first checked for protein levels and enzymatic activity for nSMase2 but were unsuccessful in finding antibodies specific enough to measure protein levels by either Western blot or microscopy. We were also unsuccessful in confidently stratifying sphingomyelinase enzymatic activity levels because the starting level was too close to the limit of detection (data not shown).

We next tested total depletion of nSMase2 using a CRISPR/Cas9 knockout system targeted against SMPD3. Deep sequencing confirmed knockout of the gene in two clonal populations (referred to as KO1 and KO2) compared to wild-type (WT) cells and the published sequence (Fig 2A). Cells were infected with JCPyV and evaluated for VP1(+) cells to ensure initial infection of the SMPD3 KO cells was unaffected by genetic manipulation compared to WT (Fig 2B). EVs concentrated from infected WT or SMPD3 KO cells were characterized by NTA, TEM, and Western. Like Figure 1, we found EVs derived from SMPD3 KO lines demonstrated an increase in particles produced per cell compared to WT but no change in size distribution (Fig 2C, Supplementary Fig 2A). TEM images also displayed typical EV morphology and similar virus-EV spatial relationships across samples (Fig 2D, Supplementary Fig 2B–D). The EVs all co-purified with appropriate EV markers and lacked the cell lysate contaminant GM130 by Western compared to WCL (Fig 2E). EV re-infection in naïve SVG-A cells demonstrated a severe defect in the infectivity of EVs derived from SMPD3 KO cells compared to WT cells (Fig 2F), confirming results seen in Figure 1. Consistent with this decrease, there was a significant reduction in the quantity of viral genomes associated with EVs derived from SMPD3 KO cells compared to WT cells (Fig 2F) but no significant reduction in viral genomes in the WCL. This demonstrates the re-infection defect is likely due to reduced virus-EV association. This may also be consistent with the notion that incomplete depletion of nSMase2 (ie chemical inhibition or knockdown as in Figure 1) does not carry the same total effect as genetic knockout. JCPyV(+) EVs were also evaluated for potential binding and/or uptake defects by flow cytometry, neither of which showed any significant changes between WT and SMPD3 KO derived EVs (binding not shown, Fig 2H). Overall these data suggest nSMase2 contributes to the JCPyV(+) EV population, though it is unlikely the only factor. Electron micrographs from SMPD3 KD or SMPD3 KO genetic backgrounds displayed images consistent with virus packaged inside EVs and associated with the exterior despite the loss of a key enzyme for exosome production (Fig 1E, Fig 2D). Further, NTA data demonstrated increased particle production (Fig 1D, Fig 2C) yet consistent EV size distribution (Supplementary Figs 1B, 2A) across genetic backgrounds. And although total KO of SMPD3 clearly produced fewer virus(+)

EVs, there was still EV-mediated infection at about 30–40% of WT. These imply proteins other than nSMase2 produce EVs important for JCPyV infection.

3.2 | Tetraspanins CD9 and CD81 significantly contribute to JCPyV(+) EV biogenesis

To identify additional proteins involved in EV biogenesis we examined a role for tetraspanins. Tetraspanins can contribute to cargo sorting, targeting to distal cells, or to an ESCRT-independent exosomal production pathway (Andreu & Yáñez-Mó, 2014; Umeda et al., 2020; Zimmerman et al., 2016). We studied their role in JCPyV(+) EV production, hypothesizing these may contribute to small EV populations in addition to nSMase2 and/or act in directing virus(+) EVs to target cells. We previously showed tetraspanins CD9 and CD81 are plentiful in SVG-A cell-derived JCPyV(+) EVs (Morris-Love et al., 2019), and used the same shRNA targeting system to deplete cells of either CD9 or CD81. Knockdown of each respective gene was confirmed by RT-qPCR (Fig 3A) and Western blot analysis to observe protein depletion (Fig 3B). Knockdown of CD9 or CD81 had no effect on initial infection (3 dpi), but significantly reduced viral spread over 9 days (Fig 3C). EVs harvested from KD versus CTRL cells were analyzed for particles produced per cell. CD9 KD cells produced more particles per cell compared to CTRL whereas CD81 KD cells produced fewer while size distributions were unchanged (Fig 3D, Supplementary Fig 3A). EV characterization by TEM established EV morphology was unchanged by genetic depletion of either protein compared to control and virus was still associated with EVs (Fig 3E, Supplementary Fig 3B–D). Western blot analysis showed co-purification with EV markers but not potential contaminants, confirming typical EV characteristics across genetic backgrounds (Fig 3F). In the EV-reinfection assay, it was noted that EVs derived from CD9 or CD81 KD cells were significantly less infectious than those derived from CTRL cells (Fig 3G). We quantified viral genomes associated with EVs using qPCR. Viral genomes in the lysate were unchanged between cell lines (Supplementary Fig 3E), but protected viral genomes associated with EVs were significantly reduced from either KD compared to CTRL (Fig 3H). This suggests the infection defect is a result of fewer virus associated EVs released from CD9 or CD81 KD compared to CTRL. We tested whether CD9 and CD81 are crucial for EV targeting in this system using the same PKH67 flow cytometry-based binding and internalization assays. No defect was detected in binding (data not shown) or uptake of virus(+) EVs (Fig 3I). Overall these data indicate a role for both CD9 and CD81 in the biogenesis of JCPyV(+) EVs in addition to nSMase2.

Endosomal sorting complexes required for transport (ESCRT) proteins do not play a significant role in JCPyV(+) EV production or EV-mediated infection.—We next asked whether an ESCRT-dependent mechanism may also produce JCPyV(+) extracellular vesicles. Using the same shRNA targeting approach as before, seven ESCRT-related proteins were targeted to produce stable single knockdown cell lines. At least one protein from each of the five protein complexes was chosen for disruption including Hepatocyte Growth factor-regulated tyrosine kinase Substrate (HGS), ALG-2-interacting protein X (ALIX), Tumor Susceptibility Gene 101 (TSG101), Vacuolar Protein Sorting (VPS) 25 homolog (VPS25), VPS20, CHarged Multivesicular body Protein 4A (CHMP4A), and VPS4A. Sufficient knockdown of gene expression was confirmed by RT-qPCR (Fig 4A). Viral spread was evaluated in each cell type at 3, 6 and 9 dpi. There was a slight

defect in the initial infection for VPS20 and VPS4A KD lines, but interestingly by 9 dpi all KD lines had increased viral spread compared to control cells (Fig 4B). Characterization of EVs produced from infected cells by nanoparticle tracking analysis demonstrated a significant increase in EVs produced per cell from the HGS KD compared to CTRL and a significant decrease from the remaining lines and no change in the overall size distributions of EVs (Fig 4C, Supplementary Fig 4A). TEM confirmed regular EV morphology and no significant changes in virus-EV spatial relationships across genetic backgrounds were noted (Fig 4D, Supplementary Fig 4B–I). Western blot analysis showed co-purification of expected EV markers and an absence of the potential cellular contaminant GM130 compared to the WCL (Fig 4E). Contrary to the expected outcome, EV re-infection of naïve SVG-A cells demonstrated either no appreciable changes or a significant increase in infectivity (Fig 4F). qPCR evaluation of protected viral genomes associated with the EVs was complimentary to the EV re-infection assay (Fig 4G), and viral genomes in the WCL had no significant changes across cell lines (Supplementary Fig 4J). Overall these data indicate an increase in released infectious viral genomes from the ESCRT KD lines compared to CTRL, suggesting that none of the ESCRT-related proteins tested play a significant role in packaging, biogenesis, or release of JCPyV(+) extracellular vesicles on their own.

3.3 | Secretory autophagy-related proteins play an important role in JCPyV(+) EV production

Secretory autophagy is an unconventional secretion method used by several pathogens (Bird et al., 2014; Pleet et al., 2018). Secretory autophagy research demonstrates major autophagy machinery are required for initial phagophore formation while specific downstream proteins target an autophagosome for secretion (Ponpuak et al., 2015; Yu et al., 2018). We hypothesized secretory autophagy may also play a role in the release of JCPyV(+) EVs and tested for autophagy markers in our EV samples by Western blot analysis. LC3-II forms puncta at membranes as it aids in the formation of autophagosomes and acts as a common marker for autophagy (Alemu et al., 2012; Yu et al., 2018). It was noted that LC3-II co-purifies with EVs derived from wild-type SVG-A cells (Supplementary Fig 5A) and EVs derived from primary choroid plexus epithelial cells (Supplementary Fig 5B) opening the possibility of a role for secretory autophagy across multiple cell types. To understand the potential contribution of secretory autophagy in JCPyV(+) EVs, we used shRNA targeted against three proteins important to downstream steps of secretory autophagy including RAB8A, RAB27A, and GRASP65. Exact mechanisms are not well-defined for each protein, but RAB27A acts in trafficking of both MVBs and amphisomes for secretion, RAB8A acts in trafficking of autophagosomes for secretion, and GRASP65 acts at an unknown phase of secreted autophagosomes and/or amphisomes (Chen et al., 2017; Dupont et al., 2011; Ejlerskov et al., 2013; Ostrowski et al., 2010; Pleet et al., 2018; Ponpuak et al., 2015). Knockdown of each protein was confirmed by RT-qPCR for gene expression (Fig 5A) and Western blot analysis for depleted protein (Fig 5B). Initial viral infection (3 dpi) was not affected by knockdown whereas viral spread over 9 days was significantly reduced for RAB8A, RAB27a, and GRASP65 KD cells compared to CTRL (Fig 5C). To test whether the decrease in spread was a result of reduced secretory autophagosomes, EVs were purified from infected cells and first characterized by NTA, TEM, and Western blot analysis.

NTA showed no significant changes in particles produced per cell or in size distributions between KDs and CTRL (Fig 5D, Supplementary Fig 5C). TEM demonstrated similar EV morphology and virus-EV spatial relationships across samples (Fig 5E, Supplementary Fig 5D–G). Western blot analysis confirmed the presence of EV markers and absence of potential organelle contaminants when compared to WCL (Fig 5F). An EV-reinfection assay revealed a significant reduction in the infectivity of EVs derived from any of the KD lines compared to the CTRL, with RAB27A presenting the most striking effect (Fig 5G). We tested whether there were fewer viral genomes associated with EVs using qPCR and found EVs derived from RAB8A, RAB27A, or GRASP65 KD lines all had significantly fewer protected viral genomes compared to EVs from CTRL cells (Fig 5H). Total genomes in the whole cell lysate were not found to differ between any cell line, indicating that fewer virions were released from KD cells (Supplementary Fig 5H). To confirm the reduced infectivity and decrease in viral genomes was not a result of a binding or internalization defect of the EVs, JCPyV(+) EVs were labeled with PKH67 and used in an uptake assay. EVs derived from RAB8A, RAB27A, or GRASP65 KD cells showed no defect in binding (data not shown) or internalization by target cells compared to controls (Fig 5I).

4 | DISCUSSION

Extracellular vesicles are a heterogeneous population that includes exosomes, microvesicles, secretory autophagosomes, and apoptotic bodies. In this article we identify crucial EV biogenesis pathways and specific proteins that produce JCPyV associated EVs. Our data are consistent with exosomes and secretory autophagosomes contributing to the JCPyV(+) EV population with specific roles for nSMase2, CD9, CD81, RAB8A, RAB27A, and GRASP65. Drug inhibition or genetic depletion of nSMase2 reduced the spread of JCPyV. Interestingly, EV production was increased from genetic depletion of nSMase2 compared to controls, but EV-mediated infection was significantly reduced. This decreased infectivity correlated with fewer encapsidated viral genomes associated with EVs from SMPD3 KO cells compared to WT meaning fewer virions are associated with EVs. We saw similar results when examining the role of tetraspanins CD9 and CD81 in the production and spread of JCPyV(+) EVs. Notably, there was a reduction in spread of virus, a significant reduction in EV-mediated infection, and a correlated significant decrease in encapsidated JCPyV genomes associated with EVs when comparing KD to CTRL conditions. Internalization of virus(+) EVs from these lines was unchanged compared to respective controls into naïve cells, suggesting genetic depletion of these proteins does not reduce targeting or uptake of EVs in this system. Re-infection and internalization assays examine the entire heterogeneous population of EVs including virus positive and negative EVs and free virus. Importantly, our previous research (see *Morris-Love et al. mBio 2019 and O'Hara et al. PLoS Pathogens 2020*) using anti-viral neutralization assays demonstrated the same heterogeneous JCPyV(+) EV populations are not inhibited by JCPyV antisera whereas purified virus is. This suggests free and exterior virus in the heterogeneous EV samples are not the major contributors to EV-mediated infection (Morris-Love et al., 2019; O'hara et al., 2020). Further advances separating virus, virus-EV subpopulations, EV labeling, and uptake assays are necessary to confirm these results. Overall, extracellular vesicles derived from SMPD3 KD or KO, CD9 KD, and CD81 KD lines harbored less infectious virus compared to controls suggesting

these proteins are important for JCPyV(+) EV biogenesis. The opposite was noted when we genetically depleted seven ESCRT-related proteins individually–viral spread was increased over time and EV-mediated infection was either increased or unchanged from the KD compared to CTRL. This suggests that JCPyV preferentially associates with nSMase2-, CD9-, and/or CD81-dependent exosomes, but not ESCRT-dependent exosomes.

Additionally, vesicles including secretory autophagosomes, MVBs, and amphisomes that undergo trafficking and/or secretion by means of RAB8A, RAB27A, or GRASP65 present important population(s) of JCPyV(+) EVs. Knockdown of either RAB8A or GRASP65 proteins demonstrated reduced JCPyV spread and significant reductions in the release of JCPyV(+) EVs with no internalization defects. This indicates that vesicles produced and/or secreted by means of RAB8A or GRASP65 contribute to JCPyV(+) EVs. Interestingly, RAB27A depletion had the most striking effect on JCPyV(+) EV-mediated infection compared to the other KDs and CTRL. Since RAB27A is important for trafficking both multivesicular bodies and amphisomes to the plasma membrane for docking and fusion we hypothesize this defect implies RAB27A has a central role in JCPyV(+) EV pathogenesis. Because these three proteins are implicated in downstream steps of an unconventional secretion method (i.e. post autophagosome formation), we hypothesize depletion of RAB8A, GRASP65, or RAB27A causes virus(+) EVs to reroute from secretion to degradation pathways, thereby reducing the number of JCPyV(+) EVs released from the cell. We chose not to knockdown canonical autophagy proteins like LC3-I and beclin-1 because directly targeting autophagy is known to inhibit infection and replication of the human polyomaviruses BKPyV and JCPyV (Basile et al., 2009; Bouley et al., 2014; Merabova et al., 2015; Sariyer et al., 2012). By knocking down RAB8A, GRASP65, and RAB27A we were able to focus on secretory pathways downstream of autophagy without affecting early events in virus infection.

Importantly, it was noted that size distribution of EVs derived from any of the KD or KO lines was unchanged by nanoparticle tracking analysis compared to controls (Supplementary Figs 1B, 2A, 3A, 4A, 5C). Similarly, electron micrographs showed comparable sizes and virus-EV relationships across samples. This infers there are multiple and/or compensatory mechanisms that produce virus(+) EVs in this system. Because each cell line is a single genetic disruption, we hypothesize when one protein is depleted other(s) are still working to produce virus(+) EVs. Likewise, the ESCRT-dependent production of exosomes relies on five complexes consisting of a myriad of proteins, many of which have overlapping functions (Henne et al., 2011; Juan & Fürthauer, 2018; Schmidt & Teis, 2012). If several other ESCRTs or pathways can compensate (or over-compensate) for the depletion and produce EVs it is possible that depleting a single ESCRT-related protein in this complex pathway is not enough to reduce the overall production of virus(+) EVs.

Additional work is needed before we can fully appreciate the biogenesis of virus(+) extracellular vesicles. Current methods study heterogeneous EV populations and may miss nuances of specific subpopulations. Differentiation will allow us to thoroughly pinpoint which population(s) are the largest contributors to infectious spread. We suspect different virus-EV subpopulations may undergo preferential uptake by target cells or *en bloc* transmission of viruses with complementary genomes. Coupled with our findings here

we could understand the biogenesis pathways important for each of these infectious EV subpopulations and determine which pathways are most critical to target in at-risk patients. Further exploration at the viral level is also needed to understand nuclear escape and viral packaging into extracellular vesicles. Understanding motifs and binding pockets within the virus structure that target it for nuclear escape and/or EV packaging would present potential druggable target(s). Overall, elucidating the exact process(es) of both viral and host-mediated mechanisms responsible for sorting, targeting, and packaging of virions into EVs is crucial to completely understand viral pathogenesis and will help us better understand how to prevent and treat debilitating JC polyomavirus infections.

Supplementary Material

Refer to Web version on PubMed Central for supplementary material.

ACKNOWLEDGEMENTS

We would like to thank all members of the Atwood lab for vigorous discussion during the course of this work. This work was supported by the National Institute of Neurological Disorders and Stroke of the National Institute of Health under grant numbers P01NS06719, R01NS043097, R35NS116836 to W.J.A.

Funding information

National Institute of Neurological Disorders and Stroke of the National Institute of Health, Grant/Award Numbers: P01NS06719, R01NS043097, R35NS116836

DATA AVAILABILITY STATEMENT

Data supporting this manuscript are available from the corresponding author under reasonable request.

REFERENCES

Abbott NJ (2002). Astrocyte-endothelial interactions and blood-brain barrier permeability. Journal of Anatomy, 200(6), 629–638. [PubMed: 12162730]

Abdulrahman BA, Abdelaziz DH, & Schatzl HM (2018). Autophagy regulates exosomal release of prions in neuronal cells. Journal of Biological Chemistry, 293(23), 8956–8968. [PubMed: 29700113]

Adang L, & Berger J (2015). Progressive multifocal leukoencephalopathy. F1000Res, 4, 1424.

Alemu EA, Lamark T, Torgersen KM, Birgisdottir AB, Larsen KB, Jain A, Olsvik H, Øvervatn A, Kirkin V, & Johansen T (2012). ATG8 family proteins act as scaffolds for assembly of the ULK complex: Sequence requirements for LC3-interacting region (LIR) motifs. Journal of Biological Chemistry, 287(47), 39275–39290. [PubMed: 23043107]

Altan-Bonnet N, Perales C, & Domingo E (2019). Extracellular vesicles: Vehicles of en bloc viral transmission. Virus Research, 265, 143–149. [PubMed: 30928427]

Andreu Z, & Yáñez-Mó M (2014). Tetraspanins in extracellular vesicle formation and function. Frontiers in Immunology, 5, 442. [PubMed: 25278937]

Assetta B, & Atwood WJ (2017). The biology of JC polyomavirus. Biological Chemistry, 398(8), 839–855. [PubMed: 28493815]

Assetta B, Maginnis MS, Gracia Ahufinger I, Haley SA, Gee GV, Nelson CDS, O'hara BA, Allen Ramdial S-AA, & Atwood WJ (2013). 5-HT2 receptors facilitate JC polyomavirus entry. Journal of Virology, 87(24), 13490–13498. [PubMed: 24089568]

Assetta B, Morris-Love J, Gee GV, Atkinson AL, O'hara BA, Maginnis MS, Haley SA, & Atwood WJ (2019). Genetic and functional dissection of the role of individual 5-HT2 receptors as entry receptors for JC polyomavirus. Cell Reports, 27(7), 1960–1966.e6. [PubMed: 31091436]

Atkinson AL, & Atwood WJ (2020). Fifty years of JC polyomavirus: A brief overview and remaining questions. Viruses, 12(9), 969. [PubMed: 32882975]

Atwood WJ, Wang L, Durham LC, Amemiya K, Traub RG, & Major EO (1995). Evaluation of the role of cytokine activation in the multiplication of JC virus (JCV) in human fetal glial cells. Journal of Neurovirology, 1(1), 40–49. [PubMed: 9222341]

Baixauli F, LÃ3Pez-Otã-N C, & Mittelbrunn M (2014). Exosomes and autophagy: Coordinated mechanisms for the maintenance of cellular fitness. Frontiers in Immunology, 5, 403. [PubMed: 25191326]

Balusu S, Van Wonterghem E, De Rycke R, Raemdonck K, Stremersch S, Gevaert K, Brkic M, Demeestere D, Vanhooren V, Hendrix A. n., Libert C, & Vandenbroucke RE (2016). Identification of a novel mechanism of blood-brain communication during peripheral inflammation via choroid plexus-derived extracellular vesicles. EMBO Molecular Medicine, 8(10), 1162–1183. [PubMed: 27596437]

Basile A, Darbinian N, Kaminski R, White MK, Gentilella A, Turco MC, & Khalili K (2009). Evidence for modulation of BAG3 by polyomavirus JC early protein. Journal of General Virology, 90(Pt 7), 1629–1640. [PubMed: 19282432]

Bekier ME, Wang L, Li J, Huang H, Tang D, Zhang X, & Wang Y (2017). Knockout of the Golgi stacking proteins GRASP55 and GRASP65 impairs Golgi structure and function. Molecular Biology of the Cell, 28(21), 2833–2842. [PubMed: 28814501]

Bello-Morales R, Praena B, De La Nuez C, Rejas MT, Guerra M, Galán-Ganga M, Izquierdo M, Calvo V, Krummenacher C, & López-Guerrero JA(2018). Role of microvesicles in the spread of herpes simplex virus 1 in oligodendrocytic cells. Journal of Virology, 92(10), e00088–18. [PubMed: 29514899]

Berger JR (2017). Classifying PML risk with disease modifying therapies. Multiple Sclerosis and Related Disorders, 12, 59–63. [PubMed: 28283109]

Bird SW, Maynard ND, Covert MW, & Kirkegaard K (2014). Nonlytic viral spread enhanced by autophagy components. PNAS, 111(36), 13081–13086. [PubMed: 25157142]

Bofill-Mas S, Formiga-Cruz M, Clemente-Casares P, Calafell F, & Girones R (2001). Potential transmission of human polyomaviruses through the gastrointestinal tract after exposure to virions or viral DNA. Journal of Virology, 75(21), 10290–10299. [PubMed: 11581397]

Bouley SJ, Maginnis MS, Derdowski A, Gee GV, O'Hara BA, Nelson CD, Bara AM, Atwood WJ, & Dugan AS (2014). Host cell autophagy promotes BK virus infection. Virology, 456–457, 87–95.

Charrin S, Jouannet S, Boucheix C, & Rubinstein E (2014). Tetraspanins at a glance. Journal of Cell Science, 127(Pt 17), 3641–3648. [PubMed: 25128561]

Chen X, Li Y, Wang C, Tang Y, Mok S-A, Tsai RM, Rojas JC, Karydas A, Miller BL, Boxer AL, Gestwicki JE, Arkin M, Cuervo AM, & Gan LI (2020). Promoting tau secretion and propagation by hyperactive p300/CBP via autophagy-lysosomal pathway in tauopathy. Molecular Neurodegeneration, 15(1), 2. [PubMed: 31906970]

Chen Y-D, Fang Y-T, Cheng Y-L, Lin CF, Hsu L-J, Wang SY, Anderson R, Chang CP, & Lin YS (2017). Exophagy of annexin A2 via RAB11, RAB8A and RAB27A in IFN-gamma-stimulated lung epithelial cells. Science Reports, 7(1), 5676.

Cinque P, Koralnik IJ, Gerevini S, Miro JM, & Price RW (2009). Progressive multifocal leukoencephalopathy in HIV-1 infection. The Lancet Infectious Diseases, 9(10), 625–636. [PubMed: 19778765]

Claude-Taupin A, Jia J, Mudd M, & Deretic V (2017). Autophagy's secret life: Secretion instead of degradation. Essays in Biochemistry, 61(6), 637–647. [PubMed: 29233874]

Colombo M, Raposo G, & Théry C (2014). Biogenesis, secretion, and intercellular interactions of exosomes and other extracellular vesicles. Annual Review of Cell and Developmental Biology, 30, 255–289.

Colombo M, Moita C, van Niel G, Kowal J, Vigneron J, Benaroch P, Manel N, Moita LF, Théry C, & Raposo G (2013). Analysis of ESCRT functions in exosome biogenesis, composition and

secretion highlights the heterogeneity of extracellular vesicles. Journal of Cell Science, 126(Pt 24), 5553–5565. [PubMed: 24105262]

Datta Chaudhuri A, Dasgheyb RM, Devine LR, Bi H, Cole RN, & Haughey NJ (2020). Stimulus-dependent modifications in astrocyte-derived extracellular vesicle cargo regulate neuronal excitability. Glia, 68(1), 128–144. [PubMed: 31469478]

Dogrammatzis C, Deschamps T, & Kalamvoki M (2019). Biogenesis of extracellular vesicles during herpes simplex virus 1 infection: Role of the CD63 tetraspanin. Journal of Virology, 93(2), e01850–18. [PubMed: 30355691]

Dupont N, Jiang S, Pilli M, Ornatowski W, Bhattacharya D, & Deretic V (2011). Autophagy-based unconventional secretory pathway for extracellular delivery of IL-1beta. EMBO Journal, 30(23), 4701–4711. [PubMed: 22068051]

Egli A, Infanti L, Dumoulin A, Buser A, Samaridis J, Stebler C, Gosert R, & Hirsch HH (2009). Prevalence of polyomavirus BK and JC infection and replication in 400 healthy blood donors. Journal of Infectious Diseases, 199(6), 837–846. [PubMed: 19434930]

Ejlerskov P, Rasmussen I, Nielsen TT, Bergström AL, Tohyama Y, Jensen PH, & Vilhardt F (2013). Tubulin polymerization-promoting protein (TPPP/p25alpha) promotes unconventional secretion of alpha-synuclein through exophagy by impairing autophagosome-lysosome fusion. Journal of Biological Chemistry, 288(24), 17313–17335. [PubMed: 23629650]

Elphick GF, Querbes W, Jordan JA, Gee GV, Eash S, Manley K, Dugan A, Stanifer M, Bhatnagar A, Kroeze WK, Roth BL, & Atwood WJ (2004). The human polyomavirus, JCV, uses serotonin receptors to infect cells. Science, 306(5700), 1380–1383. [PubMed: 15550673]

English L, Chemali M, Duron J, Rondeau C, Laplante A, Gingras D, Alexander D, Leib D, Norbury C, Lippé R, & Desjardins M (2009). Autophagy enhances the presentation of endogenous viral antigens on MHC class I molecules during HSV-1 infection. Nature Immunology, 10(5), 480–487. [PubMed: 19305394]

Fader CM, Sánchez D, Furlán M, & Colombo MI (2008). Induction of autophagy promotes fusion of multivesicular bodies with autophagic vacuoles in k562 cells. Traffic (Copenhagen, Denmark), 9(2), 230–250. [PubMed: 17999726]

Feng Y, Yu W, Li X, Lin S, Zhou Y, Hu J, & Liu X (2013). Structural insight into Golgi membrane stacking by GRASP65 and GRASP55 proteins. Journal of Biological Chemistry, 288(39), 28418–28427. [PubMed: 23940043]

Ferenczy MW, Marshall LJ, Nelson CDS, Atwood WJ, Nath A, Khalili K, & Major EO (2012). Molecular biology, epidemiology, and pathogenesis of progressive multifocal leukoencephalopathy, the JC virus-induced demyelinating disease of the human brain. Clinical Microbiology Reviews, 25(3), 471–506. [PubMed: 22763635]

Figuera-Losada M, Stathis M, Dorskind JM, Thomas AG, Bandaru VVR, Yoo SW, Westwood NJ, Rogers GW, Mcarthur JC, Haughey NJ, Slusher BS, & Rojas C (2015). Cambinol, a novel inhibitor of neutral sphingomyelinase 2 shows neuroprotective properties. PLOS One, 10(5), e0124481. [PubMed: 26010541]

Frühbeis C, Fröhlich D, Kuo WP, Amphornrat J, Thilemann S, Saab AS, Kirchhoff F, Möbius W, Goebbels S, Nave KA, Schneider A, Simons M, Klugmann M, Trotter J, & Krämer-Albers EM (2013). Neurotransmitter-triggered transfer of exosomes mediates oligodendrocyte-neuron communication. Plos Biology, 11(7), e1001604. [PubMed: 23874151]

Fujii K, Hurley JH, & Freed EO (2007). Beyond Tsg101: The role of Alix in 'ESCRTing' HIV-1. Nature Reviews Microbiology, 5(12), 912–916. [PubMed: 17982468]

Gee HY, Noh SH, Tang BL, Kim KH, & Lee MG (2011). Rescue of DeltaF508-CFTR trafficking via a GRASP-dependent unconventional secretion pathway. Cell, 146(5), 746–760. [PubMed: 21884936]

Ghosh S, Dellibovi-Ragheb TA, Kerviel A, Pak E, Qiu Q. i., Fisher M, Takvorian PM, Bleck C, Hsu VW, Fehr AR, Perlman S, Achar SR, Straus MR, Whittaker GR, De Haan CAM, Kehrl J, Altan-Bonnet G, & Altan-Bonnet N (2020). beta-coronaviruses use lysosomes for egress instead of the biosynthetic secretory pathway. Cell, 183(6), 1520–1535.e14. [PubMed: 33157038]

Giuliani F, Grieve A, & Rabouille C (2011). Unconventional secretion: A stress on GRASP. Current Opinion in Cell Biology, 23(4), 498–504. [PubMed: 21571519]

Goñi FM, & Alonso A (2009). Effects of ceramide and other simple sphingolipids on membrane lateral structure. Biochimica Et Biophysica Acta, 1788(1), 169–177. [PubMed: 18848519]

Gordón-Alonso M, Yañez-Mó M, Barreiro O, Álvarez S, Muñoz-Fernández MÁ, Valenzuela-Fernández A, & Sánchez-Madrid F (2006). Tetraspanins CD9 and CD81 modulate HIV-1-induced membrane fusion. Journal of Immunology, 177(8), 5129–5137.

Gudbergsson JM, & Johnsen KB (2019). Exosomes and autophagy: Rekindling the vesicular waste hypothesis. Journal of Cell Communication and Signaling, 13(4), 443–450. [PubMed: 31172413]

Heltweg B, Gatbonton T, Schuler AD, Posakony J, Li H, Goehle S, Kollipara R, Depinho RA, Gu Y, Simon JA, & Bedalov A (2006). Antitumor activity of a small-molecule inhibitor of human silent information regulator 2 enzymes. Cancer Research, 66(8), 4368–4377. [PubMed: 16618762]

Henne WM, Buchkovich NJ, & Emr SD (2011). The ESCRT pathway. Developmental Cell, 21(1), 77–91. [PubMed: 21763610]

Hu G, Yang L. u., Cai Y. u., Niu F, Mezzacappa F, Callen S, Fox HS, & Buch S (2016). Emerging roles of extracellular vesicles in neurodegenerative disorders: Focus on HIV-associated neurological complications. Cell Death & Disease, 7(11), e2481. [PubMed: 27882942]

Hurley JH, & Young LN (2017). Mechanisms of autophagy initiation. Annual Review of Biochemistry, 86(1), 225–244.

Im YJ, Wollert T, Boura E, & Hurley JH (2009). Structure and function of the ESCRT-II-III interface in multivesicular body biogenesis. Developmental Cell, 17(2), 234–243. [PubMed: 19686684]

Jia X, Yin Y, Chen Y, & Mao L (2021). The role of viral proteins in the regulation of exosomes biogenesis. Frontiers in Cellular and Infection Microbiology, 11, 671625. [PubMed: 34055668]

Juan T, & Fürthauer M (2018). Biogenesis and function of ESCRT-dependent extracellular vesicles. Seminars in Cell & Developmental Biology, 74, 66–77. [PubMed: 28807885]

Kerviel A, Zhang M, & Altan-Bonnet N (2021). A new infectious unit: Extracellular vesicles carrying virus populations. Annual Review of Cell and Developmental Biology, 37, 171–197.

Liu CK, & Atwood WJ (2000). Propagation and Assay of the JC Virus. SV40 Protocols. 165. New Jersey: Humana Press; p. 9–17.

Liu CK, Hope AP, & Atwood WJ The human polyomavirus, JCV, does not share receptor specificity with SV40 on human glial cells. 10.

Major EO, & Nath A (2016). A link between long-term natalizumab dosing in MS and PML: Putting the puzzle together. Neurol Neuroimmunol Neuroinflamm, 3(3), e235. [PubMed: 27213175]

Major EO, Miller AE, Mourrain P, Traub RG, De Widt E, & Sever J (1985). Establishment of a line of human fetal glial cells that supports JC virus multiplication. PNAS, 82(4), 1257–1261. [PubMed: 2983332]

Martins S. D. e. T., & Alves LR (2020). Extracellular vesicles in viral infections: Two sides of the same coin? Frontiers in Cellular and Infection Microbiology, 10, 593170. [PubMed: 33335862]

Meldolesi J (2019). Extracellular vesicles, news about their role in immune cells: Physiology, pathology and diseases. Clinical and Experimental Immunology, 196(3), 318–327. [PubMed: 30756386]

Menck K, Sönmezer C, Worst TS, Schulz M, Dihazi GH, Streit F, Erdmann G, Kling S, Boutros M, Binder C, & Gross JC (2017). Neutral sphingomyelinases control extracellular vesicles budding from the plasma membrane. Journal of Extracellular Vesicles, 6(1), 1378056. [PubMed: 29184623]

Mendes LFS, Fontana NA, Oliveira CG, Freire MCLC, Lopes JLS, Melo FA, & Costa-Filho AJ (2019). The GRASP domain in golgi reassembly and stacking proteins: Differences and similarities between lower and higher Eukaryotes. FEBS Journal, 286(17), 3340–3358. [PubMed: 31044497]

Merabova N, Sariyer IK, Saribas AS, Knezevic T, Gordon J, Turco MC, Rosati A, Weaver M, Landry J, & Khalili K (2015). WW domain of BAG3 is required for the induction of autophagy in glioma cells. Journal of Cellular Physiology, 230(4), 831–841. [PubMed: 25204229]

Moffat J, Grueneberg DA, Yang X, Kim So Y., Kloepfer AM, Hinkle G, Piqani B, Eisenhaure TM, Luo B, Grenier JK, Carpenter AE, Foo SY, Stewart SA, Stockwell BR, Hacohen N, Hahn WC, Lander ES, Sabatini DM, & Root DE (2006). A lentiviral RNAi library for human and

mouse genes applied to an arrayed viral high-content screen. Cell, 124(6), 1283–1298. [PubMed: 16564017]

Morris-Love J, Gee GV, O'hara BA, Assetta B, Atkinson AL, Dugan AS, Haley SA, & Atwood WJ (2019). JC polyomavirus uses extracellular vesicles to infect target cells. mBio, 10(2), e00379–19. [PubMed: 30967463]

Neu U, Maginnis MS, Palma AS, Ströh LJ, Nelson CDS, Feizi T, Atwood WJ, & Stehle T (2010). Structure-function analysis of the human JC polyomavirus establishes the LSTc pentasaccharide as a functional receptor motif. Cell Host Microbe, 8(4), 309–319. [PubMed: 20951965]

O'hara BA, Morris-Love J, Gee GV, Haley SA, & Atwood WJ (2020). JC virus infected choroid plexus epithelial cells produce extracellular vesicles that infect glial cells independently of the virus attachment receptor. PLOS Pathogens, 16(3), e1008371. [PubMed: 32130281]

Okonechnikov K, Golosova O, & Fursov M (2012). team U. Unipro UGENE: A unified bioinformatics toolkit. Bioinformatics, 28(8), 1166–1167. [PubMed: 22368248]

Ostrowski M, Carmo NB, Krumeich S, Fanget I, Raposo G, Savina A, Moita CF, Schauer K, Hume AN, Freitas RP, Goud B, Benaroch P, Hacohen N, Fukuda M, Desnos C, Seabra MC, Darchen F, Amigorena S, Moita LF, & Thery C (2010). Rab27a and Rab27b control different steps of the exosome secretion pathway. Nature Cell Biology, 12(1), 19–30. sup pp 1–13. [PubMed: 19966785]

Pilli M, Arko-Mensah J, Ponpuak M, Roberts E, Master S, Mandell MA, Dupont N, Ornatowski W, Jiang S, Bradfute SB, Bruun JA, Hansen TE, Johansen T, & Deretic V (2012). TBK-1 promotes autophagy-mediated antimicrobial defense by controlling autophagosome maturation. Immunity, 37(2), 223–234. [PubMed: 22921120]

Pleet ML, Branscome H, Demarino C, Pinto DO, Zadeh MA, Rodriguez M, Sariyer IK, El-Hage N, & Kashanchi F (2018). Autophagy, EVs, and infections: A perfect question for a perfect time. Frontiers in Cellular and Infection Microbiology, 8, 362. [PubMed: 30406039]

Ponpuak M, Mandell MA, Kimura T, Chauhan S, Cleyrat C, & Deretic V (2015). Secretory autophagy. Current Opinion in Cell Biology, 35, 106–116. [PubMed: 25988755]

Rabouille C (2017). Pathways of unconventional protein secretion. Trends in Cell Biology, 27(3), 230–240. [PubMed: 27989656]

Rajendran L, Honsho M, Zahn TR, Keller P, Geiger KD, Verkade P, & Simons K (2006). Alzheimer's disease beta-amyloid peptides are released in association with exosomes. PNAS, 103(30), 11172–11177. [PubMed: 16837572]

Santiana M, Ghosh S, Ho BA, Rajasekaran V, Du W. -L. i., Mutsafi Y, De Jésus-Diaz DA, Sosnovtsev SV, Levenson EA, Parra GI, Takvorian PM, Cali A, Bleck C, Vlasova AN, Saif LJ, Patton JT, Lopalco P, Corcelli A, Green KY, & Altan-Bonnet N (2018). Vesicle-cloaked virus clusters are optimal units for inter-organismal viral transmission. Cell Host Microbe, 24(2), 208–220.e8. [PubMed: 30092198]

Sariyer IK, Merabova N, Patel PK, Knezevic T, Rosati A, Turco MC, & Khalili K (2012). Bag3-induced autophagy is associated with degradation of JCV oncoprotein, T-Ag. Plos One, 7(9), e45000. [PubMed: 22984599]

Schmidt O, & Teis D (2012). The ESCRT machinery. Current Biology, 22(4), R116–R120. [PubMed: 22361144]

Schwab A, Meyering SS, Lepene B, Iordanskiy S, Van Hoek ML, Hakami RM, & Kashanchi F (2015). Extracellular vesicles from infected cells: potential for direct pathogenesis. Frontiers in Microbiology, 6, 1132. [PubMed: 26539170]

Shamseddine AA, Airola MV, & Hannun YA (2015). Roles and regulation of neutral sphingomyelinase-2 in cellular and pathological processes. Advances in Biological Regulation, 57, 24–41. [PubMed: 25465297]

Snead WT, Hayden CC, Gadok AK, Zhao C, Lafer EM, Rangamani P, & Stachowiak JC (2017). Membrane fission by protein crowding. Proceedings of the National Academy of Sciences of the United States of America, 114(16), E3258–E67. [PubMed: 28373566]

Son SM, Cha MY, Choi H, Kang S, Choi H, Lee MS, Park S. A. h, & Mook-Jung I (2016). Insulin-degrading enzyme secretion from astrocytes is mediated by an autophagy-based unconventional secretory pathway in Alzheimer disease. Autophagy, 12(5), 784–800. [PubMed: 26963025]

Soria FN, Pampliega O, Bourdenx M, Meissner WG, Bezard E, & Dehay B (2017). Exosomes, an unmasked culprit in neurodegenerative diseases. Frontiers in Neuroscience, 11, 26. [PubMed: 28197068]

Stachowiak JC, Schmid EM, Ryan CJ, Ann HS, Sasaki DY, Sherman MB, Geissler PL, Fletcher DA, & Hayden CC (2012). Membrane bending by protein-protein crowding. Nature Cell Biology, 14(9), 944–949. [PubMed: 22902598]

Stoorvogel W, Kleijmeer MJ, Geuze HJ, & Raposo G (2002). The biogenesis and functions of exosomes. Traffic (Copenhagen, Denmark), 3(5), 321–330. [PubMed: 11967126]

Ströh LJ, Maginnis MS, Blaum BS, Nelson CDS, Neu U, Gee GV, O'hara BA, Motamedi N, Dimaio D, Atwood WJ, & Stehle T (2015). The greater affinity of JC polyomavirus capsid for alpha2,6-linked lactoseries tetrasaccharide c than for other sialylated glycans is a major determinant of infectivity. Journal of Virology, 89(12), 6364–6375. [PubMed: 25855729]

Tancini B, Buratta S, Sagini K, Costanzi E, Delo F, Urbanelli L, & Emiliani C (2019). Insight into the role of extracellular vesicles in lysosomal storage disorders. Genes (Basel), 10(7), 510. [PubMed: 31284546]

Tang D, Yuan H, & Wang Y (2010). The role of GRASP65 in Golgi cisternal stacking and cell cycle progression. Traffic (Copenhagen, Denmark), 11(6), 827–842. [PubMed: 20214750]

Théry C, Zitvogel L, & Amigorena S (2002). Exosomes: Composition, biogenesis and function. Nature Reviews Immunology, 2(8), 569–579.

Torres C (2020). Evolution and molecular epidemiology of polyomaviruses. Infection, Genetics and Evolution, 79, 104150.

Trajkovic K, Hsu C, Chiantia S, Rajendran L, Wenzel D, Wieland F, Schwille P, BrüGger B, & Simons M (2008). Ceramide triggers budding of exosome vesicles into multivesicular endosomes. Science, 319(5867), 1244–1247. [PubMed: 18309083]

Umeda R, Satouh Y, Takemoto M, Nakada-Nakura Y, Liu K, Yokoyama T, Shirouzu M, Iwata S. o., Nomura N, Sato K, Ikawa M, Nishizawa T, & Nureki O (2020). Structural insights into tetraspanin CD9 function. Nature Communication, 11(1), 1606.

Urbanelli L, Buratta S, Tancini B, Sagini K, Delo F, Porcellati S, & Emiliani C (2019). The role of extracellular vesicles in viral infection and transmission. Vaccines (Basel), 7(3), 102. [PubMed: 31466253]

Van Der Grein SG, Defourny KAY, Slot EFJ, & Nolte-'T Hoen ENM (2018). Intricate relationships between naked viruses and extracellular vesicles in the crosstalk between pathogen and host. Seminars in Immunopathology, 40(5), 491–504. [PubMed: 29789863]

Van Niel G, D'angelo G, & Raposo G (2018). Shedding light on the cell biology of extracellular vesicles. Nature Reviews Molecular Cell Biology, 19(4), 213–228. [PubMed: 29339798]

Van Niel G, Charrin S, Simoes S, Romao M, Rochin L, Saftig P, Marks MS, Rubinstein E, & Raposo G (2011). The tetraspanin CD63 regulates ESCRT-independent and -dependent endosomal sorting during melanogenesis. Developmental Cell, 21(4), 708–721. [PubMed: 21962903]

Veenendaal T, Jarvela T, Grieve AG, Van Es JH, Linstedt AD, & Rabouille C (2014). GRASP65 controls the cis Golgi integrity in vivo. Biology Open, 3(6), 431–443. [PubMed: 24795147]

Vella LJ, Sharples RA, Lawson VA, Masters CL, Cappai R, & Hill AF (2007). Packaging of prions into exosomes is associated with a novel pathway of PrP processing. Journal of Pathology, 211(5), 582–590. [PubMed: 17334982]

Verderio C, Gabrielli M, & Giussani P (2018). Role of sphingolipids in the biogenesis and biological activity of extracellular vesicles. Journal of Lipid Research, 59(8), 1325–1340. [PubMed: 29853528]

Witwer KW, Soekmadji C, Hill AF, Wauben MH, Buzás EI, Di Vizio D, Falcon-Perez JM, Gardiner C, Hochberg F, Kurochkin IV, Lötvall J, Mathivanan S, Nieuwland R, Sahoo S, Tahara H, Torrecilhas AC, Weaver AM, Yin H, Zheng L, … Théry C (2017). Updating the MISEV minimal requirements for extracellular vesicle studies: Building bridges to reproducibility. Journal of Extracellular Vesicles, 6(1), 1396823. [PubMed: 29184626]

Wollert T, & Hurley JH (2010). Molecular mechanism of multivesicular body biogenesis by ESCRT complexes. Nature, 464(7290), 864–869. [PubMed: 20305637]

Xiang Y. i., & Wang Y (2010). GRASP55 and GRASP65 play complementary and essential roles in Golgi cisternal stacking. Journal of Cell Biology, 188(2), 237–251. [PubMed: 20083603]

Xu R, Rai A, Chen M, Suwakulsiri W, Greening DW, & Simpson RJ (2018). Extracellular vesicles in cancer - implications for future improvements in cancer care. Nature Reviews Clinical Oncology, 15(10), 617–638.

You Y, & Ikezu T (2019). Emerging roles of extracellular vesicles in neurodegenerative disorders. Neurobiology of Disease, 130, 104512. [PubMed: 31229685]

Yu L. i., Chen Y, & Tooze SA (2018). Autophagy pathway: Cellular and molecular mechanisms. Autophagy, 14(2), 207–215. [PubMed: 28933638]

Zhang M, & Schekman R (2013). Cell biology. Unconventional secretion, unconventional solutions. Science, 340(6132), 559–561. [PubMed: 23641104]

Zhang M, Kenny SJ, Ge L, Xu K. e., & Schekman R (2015). Translocation of interleukin-1beta into a vesicle intermediate in autophagy-mediated secretion. Elife, 4, e11205. [PubMed: 26523392]

Zhang X, & Wang Y (2020). Nonredundant roles of GRASP55 and GRASP65 in the Golgi apparatus and beyond. Trends in Biochemical Sciences, 45(12), 1065–1079. [PubMed: 32893104]

Zhang X, Wang L, Ireland SC, Ahat E, Li J, Bekier ME, Zhang Z, & Wang Y (2019). GORASP2/GRASP55 collaborates with the PtdIns3K UVRAG complex to facilitate autophagosome-lysosome fusion. Autophagy, 15(10), 1787–1800. [PubMed: 30894053]

Zhang X, Wang L, Lak B, Li J, Jokitalo E, & Wang Y (2018). GRASP55 senses glucose deprivation through O-GlcNAcylation to promote autophagosome-lysosome fusion. Developmental Cell, 45(2), 245–261.e6. [PubMed: 29689198]

Zhang Y, & Seemann J (2021). Rapid degradation of GRASP55 and GRASP65 reveals their immediate impact on the Golgi structure. Journal of Cell Biology, 220(1).

Zimmerman B, Kelly B, Mcmillan BJ, Seegar TCM, Dror RO, Kruse AC, & Blacklow SC (2016). Crystal structure of a full-length human tetraspanin reveals a cholesterol-binding pocket. Cell, 167(4), 1041–1051.e11. [PubMed: 27881302]

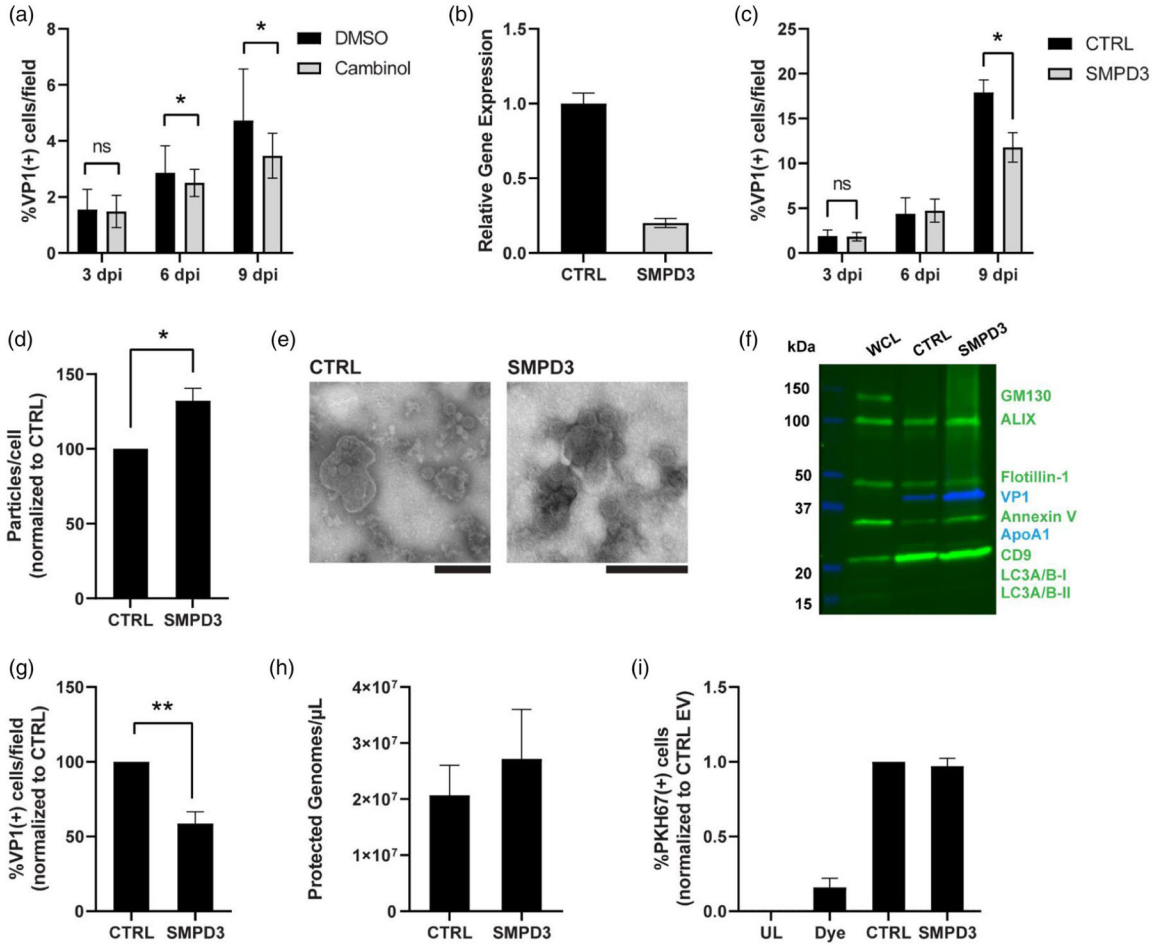

FIGURE 1.

Disruption of neutral sphingomyelinase 2 reduces EV mediated spread of JCPyV. (A) SVG-A cells were infected with JCPyV then treated with either DMSO vehicle control or 10 μM cambinol. Spread of virus was evaluated at 3, 6, and 9 days post infection (dpi) for %VP1(+) cells. (B) shRNA targeting SMPD3 or an empty vector was used to produce control (CTRL) or SMPD3 knockdown (KD) cell lines. RT-qPCR was used to confirm sufficient knockdown of gene expression. (C) CTRL or SMPD3 KD cells were infected with virus and viral spread was evaluated at 3, 6, and 9 dpi. (D) Nanoparticle tracking analysis (NTA) was used to evaluate the concentration of particles/mL and compared to the initial cell count the supernatant was harvested from to determine particles produced per cell. Values are compared to CTRL. (E) Transmission electron microscopy (TEM) was used to evaluate virus(+) EVs derived from CTRL and SMPD3 KD cells. Scale bars are 200 nm. (F) Western blot analysis was used to evaluate relative purity of EV samples. 7.5 μg of whole cell lysate (WCL), EVs derived from CTRL and SMPD3 KD cells were run and probed for common EV markers (ALIX, Flotillin-1, Annexin V, CD9, LC3A/B-I and -II), potential contaminants (GM130 and ApoA1), and the major viral capsid protein VP1. ApoA1 was not detected in any lane. (G) Virus(+) EVs derived from CTRL or SMPD3 KD lines were used to infect naïve wild-type SVG-A cells and evaluated for infection after 3 days. (H) qPCR was used to evaluate the quantity of viral genomes associated with EVs derived from CTRL or SMPD3

KD cells. (I) EVs were labeled with PKH67 and used in an uptake assay. Internalization of EVs was determined by flow cytometry before and after a trypan blue quench. Percent PKH67(+) cells from each sample type were normalized to the CTRL EVs for presentation. Only post-trypan blue quench values are shown

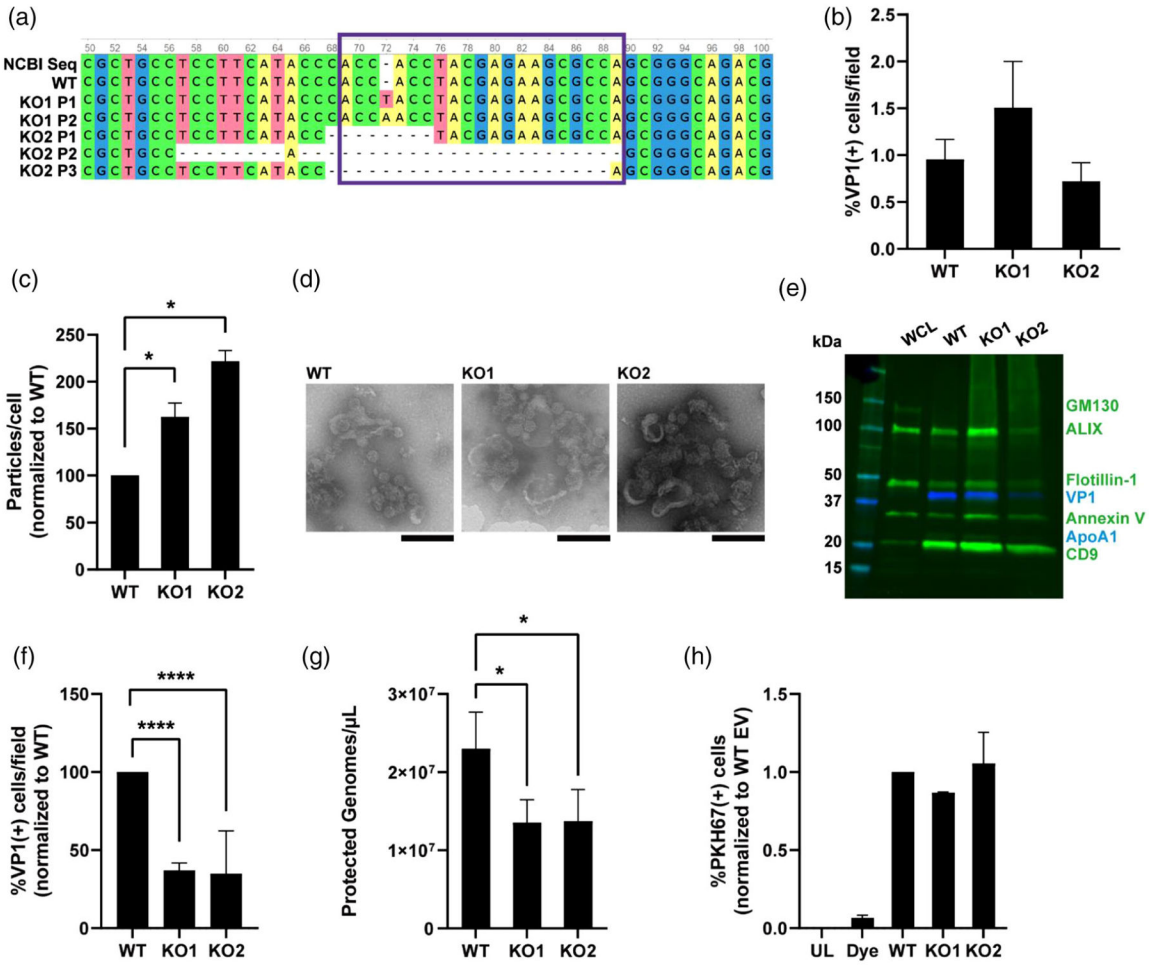

FIGURE 2.

CRISPR/Cas9 knockout of SMPD3 decreases JCPyV(+) EV. (A) SVG-A cells were targeted with a CRISPR/Cas9 system to knockout SMPD3. Two clones were grown and sequenced against wild-type SVG-A cells. Sequencing results around the induced mutations are presented against the recorded NCBI sequence for SMPD3. The purple box represents the target sequence carried by the guideRNA. Populations (P#) represent CRISPR variants detected during next generation sequencing, with two major populations detected for KO1 and three for KO2. Graphic created in Unipro UGENE (Okonechnikov et al., 2012). (B) Wild-type (WT) or knockout (KO) cells were infected with JCPyV and evaluated for initial viral infection at 3 dpi. (C) EVs were evaluated for particles produced per cell by comparing the NTA data to the initial cell count. Values are compared to WT. (D) Negative stains paired with TEM was used to evaluate virus(+) EVs derived from WT, KO1, and KO2 cells. Scale bars are 200 nm. (E) Western blot analysis was used to see presence of EV markers and absence of potential contaminants across all EVs compared to whole cell lysate (WCL). 1.8 μg of each sample was probed for common EV markers (ALIX, Flotillin-1, Annexin V, CD9), potential contaminants (GM130 and ApoA1), and the major viral capsid protein VP1. ApoA1 was not detected in any lane. (F) Virus(+) EVs derived from each cell line were used to infect naïve wild-type SVG-A cells and evaluated for infection after 3 days. (G) qPCR

was used to evaluate the quantity of viral genomes associated with EVs derived from each line. (H) Infectious EVs derived from each cell line were labeled with PKH67 and used in an uptake assay. Internalization of EVs was determined by flow cytometry before and after a trypan blue quench. Percent PKH67(+) cells from each sample type were normalized to the WT EVs for presentation, showing only post-trypan blue quench values. Graph represents two independent experiments in triplicate

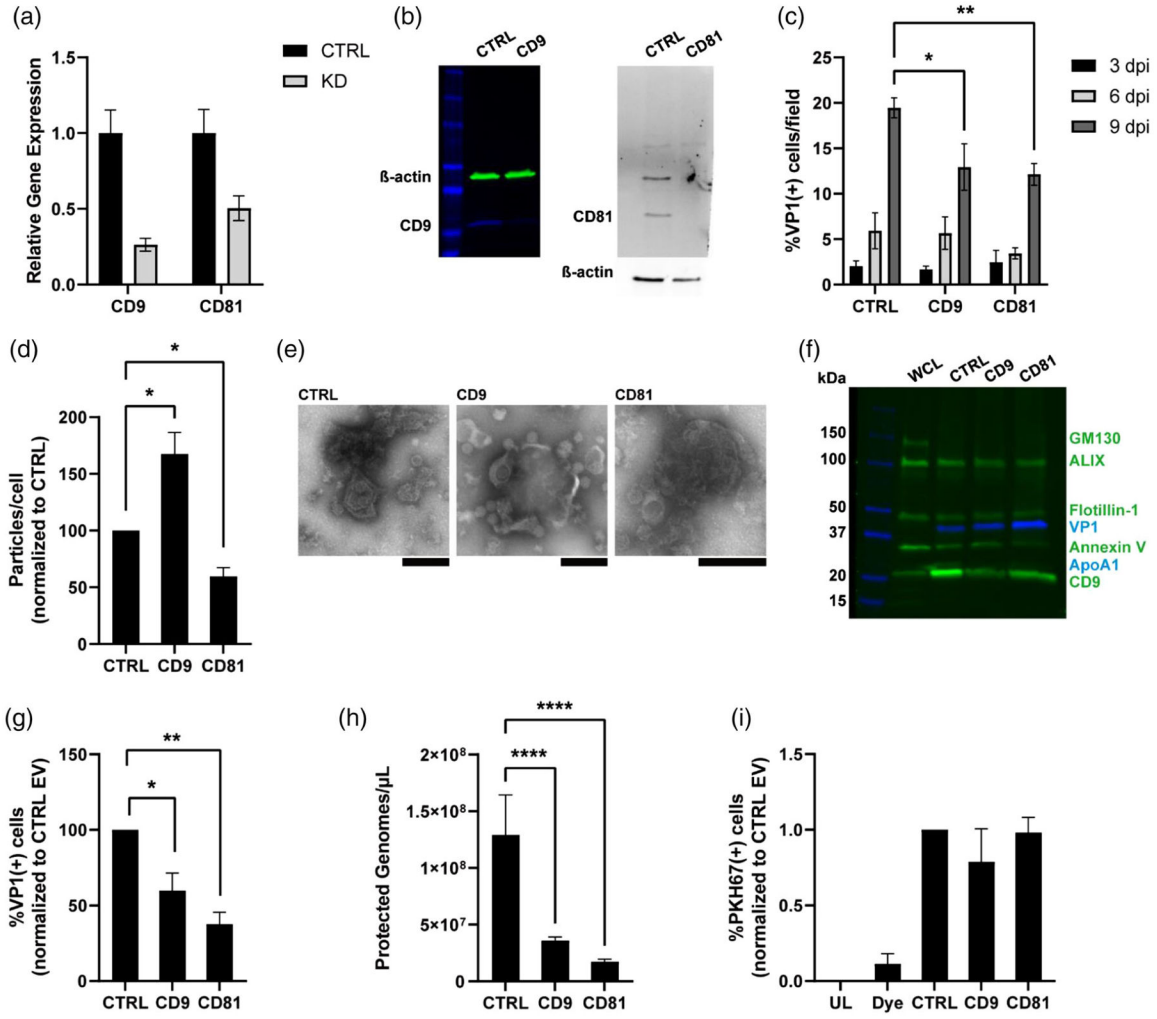

FIGURE 3.

Knockdown of tetraspanin CD9 or CD81 releases fewer infectious EVs. (A) SVG-A cells were targeted with shRNA against CD9 or CD81. RT-qPCR was used to confirm sufficient knockdown compared to control line. (B) Depletion of respective proteins (left: CD9 KD, right: CD81 KD) was confirmed using Western blot analysis with antibodies against CD9, CD81, and β-actin. (C) Spread of virus was evaluated at 3, 6, and 9 dpi in knockdown versus control cells. (D) EVs harvested from infected cells were assessed via NTA and initial cell counts for particles produced per cell. Each was normalized to control. (E) EV morphology and spatial relationship to JCPyV particles was observed by TEM using a negative stain. Scale bars are 200 nm. (F) EVs were characterized by Western blot analysis and probed for common EV markers (ALIX, Flotillin-1, Annexin V, and CD9), potential contaminants (GM130 and ApoA1), and the viral protein VP1. ApoA1 was not detected in any lane. (G) EVs derived from CTRL or either knockdown line were used in an EV-reinfection assay with infectivity evaluated at 3 dpi for %VP1(+) cells. Values are normalized to control for representation. (H) Viral genomes associated with EVs derived from each line were calculated using qPCR. (I) EVs were labeled with PKH67 and tested for uptake potential by flow cytometry before and after a trypan blue quench. Percent PKH67(+) cells (internalized

EVs) post trypan blue quench are shown compared to the control for each sample. Graph represents two independent experiments run in triplicate

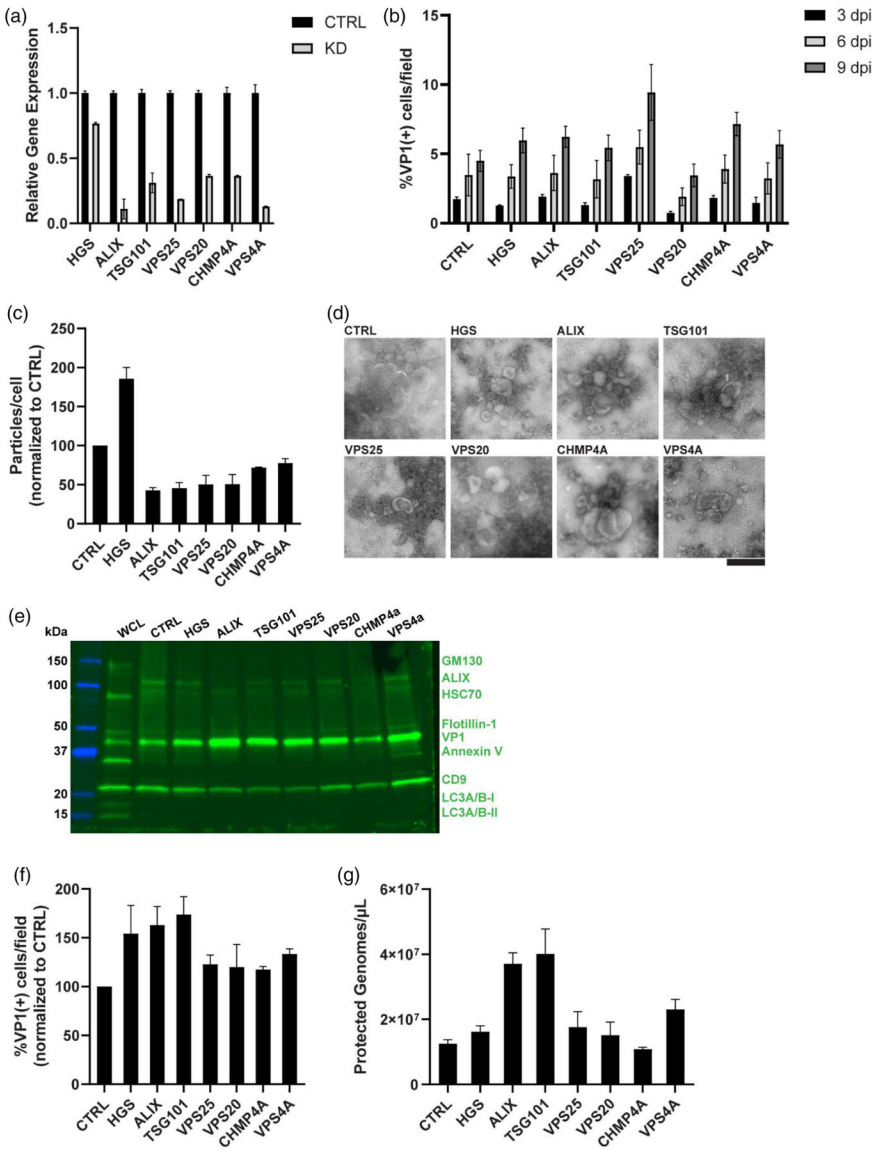

FIGURE 4.

Single knockdown of ESCRT related proteins does not affect JCPyV(+) EV production. (A) shRNA was used to knockdown seven separate ESCRT-related proteins. Gene knockdown was confirmed by RT-qPCR for the respective gene compared to control cells. (B) Each knockdown line was infected with JCPyV to evaluate spread of virus over 3, 6, and 9 days. (C) Particles produced per cell was determined using NTA for EV particle concentration compared to the initial cell count. Values are normalized to control. (D) TEM was used to examine EV morphology and spatial relationship to JCPyV particles using a negative stain. Scale bar = 200 nm. (E) EVs derived from each cell line were characterized by Western blot analysis and probed for EV markers (ALIX, HSC70, Flotillin-1, Annexin V, CD9, LC3A/B-I and -II), potential EV contaminants (GM130), and the viral protein VP1. ApoA1 was tested on a separate Western and not detected in any lane. (F) Virus(+) EVs derived from each cell line was evaluated for re-infection potential at 3 dpi. Percent VP1(+) cells were each

normalized to control. (G) qPCR was used to determine the quantity of viral genomes associated with EVs

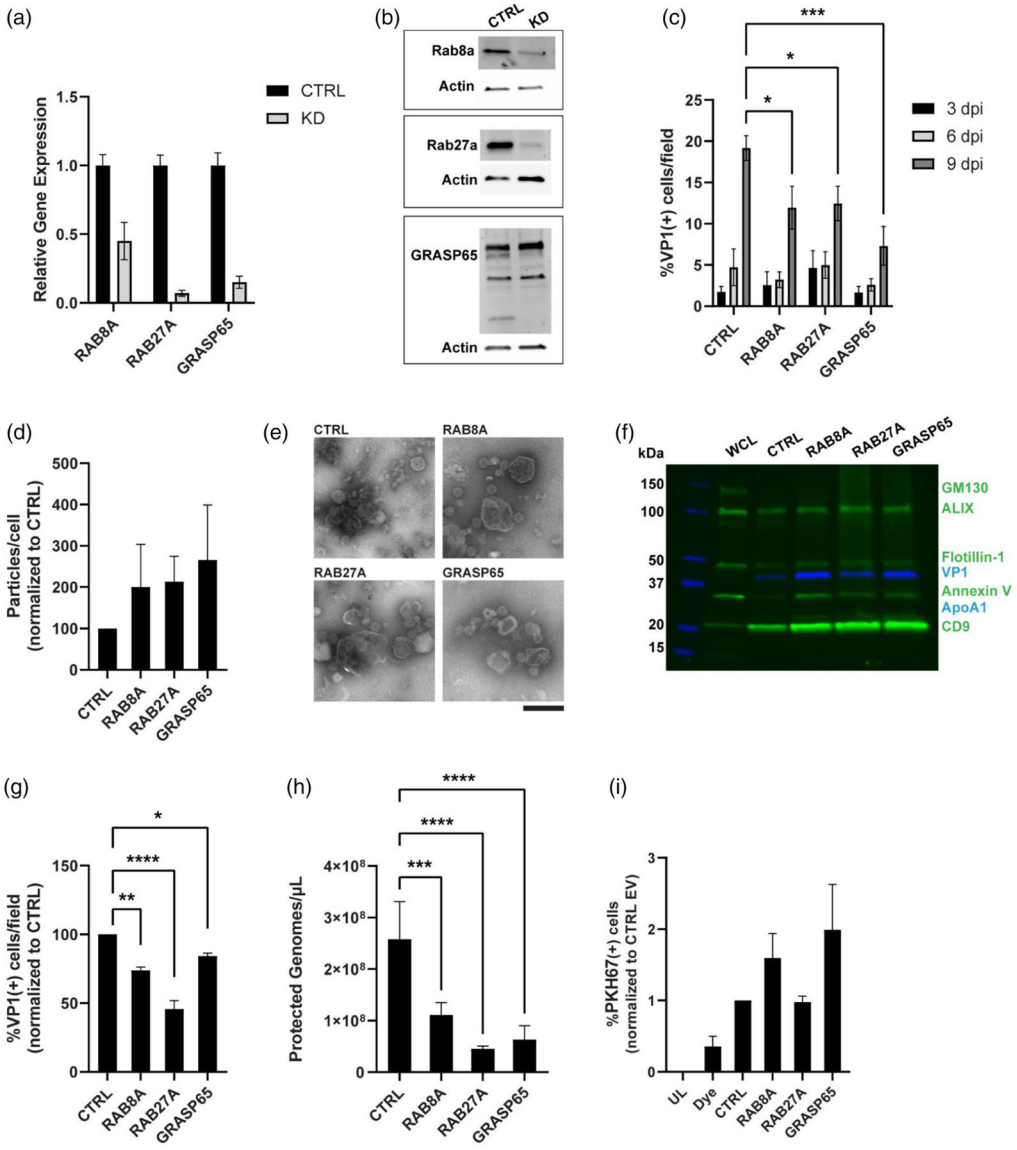

FIGURE 5.

Secretory autophagy related proteins contribute to infectious JCPyV(+) EV populations. (A) RT-qPCR was used to confirm sufficient knockdown of RAB8A, RAB27A, or GRASP65 compared to control cells. (B) Depletion of respective proteins was confirmed using Western blot analysis using antibodies against RAB8A, RAB27A, GRASP65, and β-actin. Top panel shows CTRL vs RAB8A KD, middle panel shows CTRL vs RAB27A KD, bottom panel shows CTRL vs GRASP65 KD. (C) Spread of JCPyV was evaluated at 3, 6, and 9 dpi in KD versus CTRL cells. (D) Particles produced per cell for each EV population was assessed using NTA against the initial cell count. Each is normalized to control. (E) EV morphology and spatial relationship to JCPyV particles was observed by TEM. Scale bar = 200 nm. (F) EV characterization via Western blot analysis with common EV markers (ALIX, Flotillin-1, Annexin V, and CD9), potential contaminants (GM130 and ApoA1), and the viral protein VP1 was performed for each EV against WCL. ApoA1 was not detected in any lane. (G)

EVs were used to infect naïve SVG-A cells with infectivity evaluated at 3 dpi for %VP1(+) cells. Values are normalized to control for representation. (H) Viral genomes associated with EVs derived from each line were calculated using absolute qPCR. (I) EVs were labeled with PKH67 and tested for uptake potential by flow cytometry before and after a trypan blue quench. Percent PKH67(+) cells (internalized EVs) post trypan blue quench are shown compared to the control EVs for each sample